New Miniaturized Wristed Instruments for In-Office Endoscopic Laser Surgery

by

Alex J. Chiluisa Coello

A Thesis

Submitted to the Faculty

of the

WORCESTER POLYTECHNIC INSTITUTE

In partial fulfillment of the requirements for the

Degree of Doctor of Philosophy

in

Robotics Engineering

May 2024

APPROVED BY:

_____

Prof. Loris Fichera
Department of Robotics Engineering, Worcester Polytechnic Institute

_____

Prof. Haichong Zhang
Department of Robotics Engineering, Worcester Polytechnic Institute

_____

Prof. Nicholas Bertozzi
Department of Robotics Engineering, Worcester Polytechnic Institute

_____

Dr. Thomas Carroll
Department of Otolaryngology–Head and Neck Surgery, Harvard Medical School

Abstract

Endoscopic laser surgery is emerging as a promising alternative for the treatment of various pathological conditions that affect the vocal folds. Compared to traditional laryngeal surgery, which requires general anesthesia and hospitalization, in-office surgery is faster, less expensive, and it can be performed without general anesthesia. Despite their documented benefits, in-office laryngeal procedures are still underutilized because of how challenging they can be to perform with available instrumentation. Clinically available instruments (endoscopes and optical fibers) present limited dexterity, which in turn greatly limits surgical access. This dissertation introduces a comprehensive analysis, conceptualization, and implementation of a steerable optical fiber to address these challenges, aiming to enhance surgical precision and extend reach to previously inaccessible regions within the human larynx. First, we establish a simulation framework to identify currently inaccessible regions within the larynx during endoscopic laser surgeries. This framework utilizes three-dimensional models of the human larynx generated from microtomography x-ray scans and formulates the kinematic characterization of the endoscope. Then, we introduce a steerable optical fiber to amplify a physicians reach within the larynx. This work involves designing and modeling a steerable sheath utilizing an asymmetric notch pattern, which provides three independent degrees of freedom (DoF) for precise laser aiming. A control mechanism is also developed to enable single-handed operation of the steerable fiber, minimizing alterations to the clinical setting for in-office laser surgery. Experimental results demonstrate that the proposed device substantially enhances surgical access compared to current clinical fibers. The dissertation concludes by discussing future avenues of research, including further clinical validation and refinement of control mechanisms.

Acknowledgements

I extend my deepest gratitude to my advisor, Dr. Loris Fichera, whose patient guidance, and expertise have been invaluable throughout this journey. Your mentorship went beyond the academic field. It has not only shaped this thesis but also helped me to acquire new skills for my future professional life.

I am profoundly thankful to my thesis committee, Professor Nicholas Bertozzi, Dr. Thomas Carroll, and Dr. Haichong Zhang, for the crucial scientific advice that contributed to the culmination of this project. My deepest gratitude to Dr. Thomas Carroll whose medical expertise and feedback were fundamental in the execution of the project.

To my friends and colleagues in the Comet Lab, your camaraderie, insights, and collaboration have made this research both enjoyable and rewarding. I am grateful for the stimulating discussions, shared challenges, and the sense of community that we have fostered together. A special thank you to my friends in Ecuador, who despite the distance have accompanied me and helped me through difficult times.

To my family for their unconditional love, encouragement, and support. Their unwavering belief in me has been the keystone of my academic pursuits. Thank you to my parents, Gustavo and Lupe for keeping me motivated and checking that I was doing well far away from home, and to my siblings, Sharon, Rodrigo and Jorge, for always being there, listening to me and making me laugh when things were hard.

To my wife, Salome, whose support, patience, and understanding have been my anchor throughout this journey. Your love and encouragement have sustained me through the long hours and challenging moments.

Finally, I would like to express my appreciation to all those who have contributed, directly or indirectly, to this work. Your contributions, whether through discussions, feedback, or encouragement, have been invaluable. Thank you for being part of this journey.

TABLE OF CONTENTS

List of Tables

List of Figures

CHAPTER 1

INTRODUCTION

1.1 Motivation

Benign lesions of the larynx, such as *cysts*, *nodules*, and *papillomas*, are prevalent worldwide affecting 1 in 40 adults [1, 2, 3, 4]. If left untreated, these lesions can lead to various complications, including speech impairment, difficulty in swallowing, and in more severe cases, respiratory obstruction. The traditional approach for treating these lesions involves surgical resection in the operating room (OR) under general anesthesia [5, 6].

In recent years, a new surgical approach for the treatment of these lesions is starting to emerge, namely, office-based laser surgery [7, 8, 9, 10]. Fig. 1.1 illustrates how these procedures work. In contrast to traditional procedures, general anesthesia is no longer required, and patients undergo surgery awake while sitting on an examination chair. The operating physician introduces a flexible endoscope through one of the nostrils and passes a laser fiber through the operating channel of the endoscope to apply laser pulses and thermally necrotize the affected tissue. The main benefits of office-based procedures include shorter recovery time and lower costs compared to traditional surgical management [8, 9, 10, 11, 12, 13, 14]. Additionally, by removing the need for general anesthesia, the office-based approach expands the pool of individuals eligible for laryngeal surgery.

Despite these benefits, office-based procedures remain underutilized due to the limitations of the available instrumentation. The laser fibers used to deliver treatment only emit light forward following the longitudinal axis of the fiber, thus, forcing physicians to control the laser aiming indirectly by bending the endoscope, as shown in Fig. 1.2 (a).

Figure 1.1: *Office-based laryngeal surgery of the vocal folds. Patients undergo surgery awake while sitting on the examination chair. The surgeon inserts a flexible endoscope through the nose to access the larynx. Right-handed physicians typically hold the endoscope with their right hand; the left hand rests on the patient's face to stabilize the endoscope and to feel any patient movements.*

Additionally, the lack of distal articulation of laser fibers limits the maneuverability of the fiber to reach lesions within the larynx. For instance, it is not uncommon for a tumor to develop directly beneath the free edge of the vocal folds [15, 16, 17], a location where aiming the laser fiber is challenging as Fig. 1.2 (b) shows. In this case, patients are not eligible for an in-office surgery [18], and they need to be resorted to the operating room. Finally, the procedure can become disorienting for the surgeon because they continuously need to adjust the field of view while aiming the laser fiber [19].

This thesis aims to contribute to the progress of treating laryngeal lesions by addressing the limitations described above. The goal is to create a novel laser probe with an independent distal steering mechanism to enhance maneuverability and control of the laser fiber during office-based procedures. As we shall see in the following sections, we

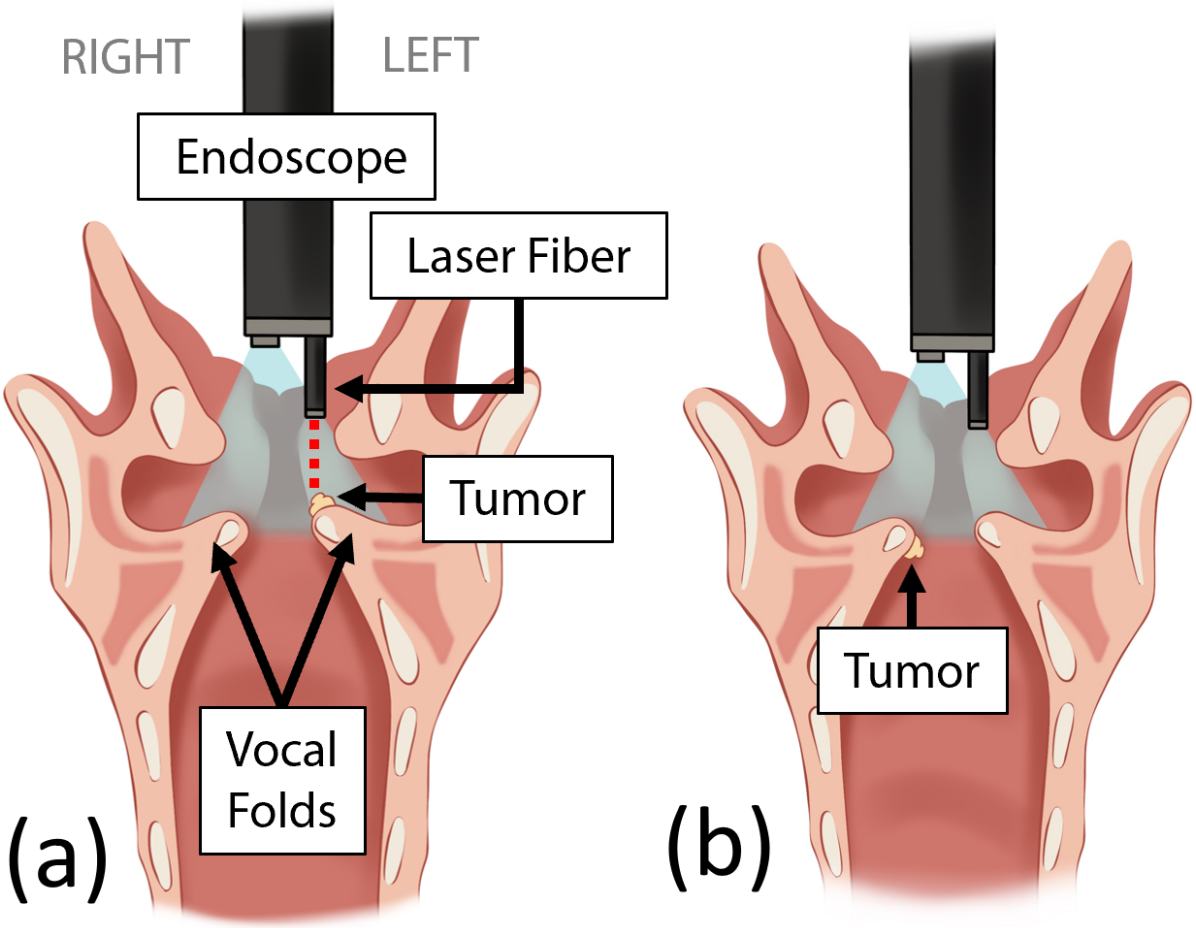

Figure 1.2: *Frontal cut of the human larynx illustrating the approach used in office-based vocal folds laser surgery: (a) An endoscope is deployed in the proximity of the vocal folds and a laser fiber is used to thermally treat diseased tissue. The blue cone represents the field of view of the endoscopic camera, while the dashed red line shows the line of sight between the laser fiber and the target tumor. (b) In some instances, a tumor may grow below the free edge of one of the vocal folds, where the laser fiber cannot be easily aimed to. Patients who present with disease in unfavorable locations are not candidates for office treatment.*

propose a solution that combines a thin optical fiber with an innovative Nickel-Titanium (Nitinol) sheath, incorporating a distal flexure-based articulation mechanism that can simply actuated with a single pull-wire [20, 21]. This instrument enables panning and tilting of the laser fiber facilitating laser aiming control in office-based surgery.

1.2 Clinical Relevance

One of the various clinical conditions that could benefit from the innovative features of the laser probe is Recurrent Respiratory Papillomatosis (RRP). RRP is characterized by the recurring growth of benign tumors inside the larynx, caused by the human papillomavirus infection, affecting nearly 20,000 individuals in the United States at any time [22, 23]. To date, no definitive treatment for RRP exists, and the only available management strategy involves repeated surgeries aimed to contain the spread of the disease [24, 25]. Typically, RRP patients visit the operating room at least once a year for the rest of their lives, and more severe cases may require surgery every few weeks [26]. The requirement of frequent surgeries not only compromises patients' quality of life but also imposes a substantial financial burden, with average lifetime treatment costs exceeding $200,000 [27]. An alternative to mitigate this cost is transitioning from traditional surgical approaches to office-based outpatient procedures. Previous studies have demonstrated the clinical feasibility of treating RRP endoscopically in the office using lasers [28, 29, 30, 31, 32], and a cost analysis revealed savings of nearly $6,000 per procedure [10, 33]. However, one in three RRP patients remains ineligible for office-based treatment because they present with disease in locations beyond the reach of the laser fiber [18]. By adding distal bending to the laser delivery fibers, the new probe could potentially allow physicians to achieve more extensive coverage of the laryngeal cavity leading to a reduction of unnecessary surgical procedures for many RRP patients.

1.3 Laser Aiming Systems for Endoscopic Surgery

Over the past years, numerous studies have explored the development of miniaturized laser-aiming systems for surgeries in confined spaces, such as the human larynx [34]. Fig. 1.3 summarizes existing approaches into two main categories; On the top row are mirror-based systems: a controlled motion of miniaturized mirrors, typically operated by piezoelectric motors, is used to deflect the path of the free laser beam [35, 36, 37, 38]. On the other hand, in the bottom row, there are fiber delivery systems that eliminate the

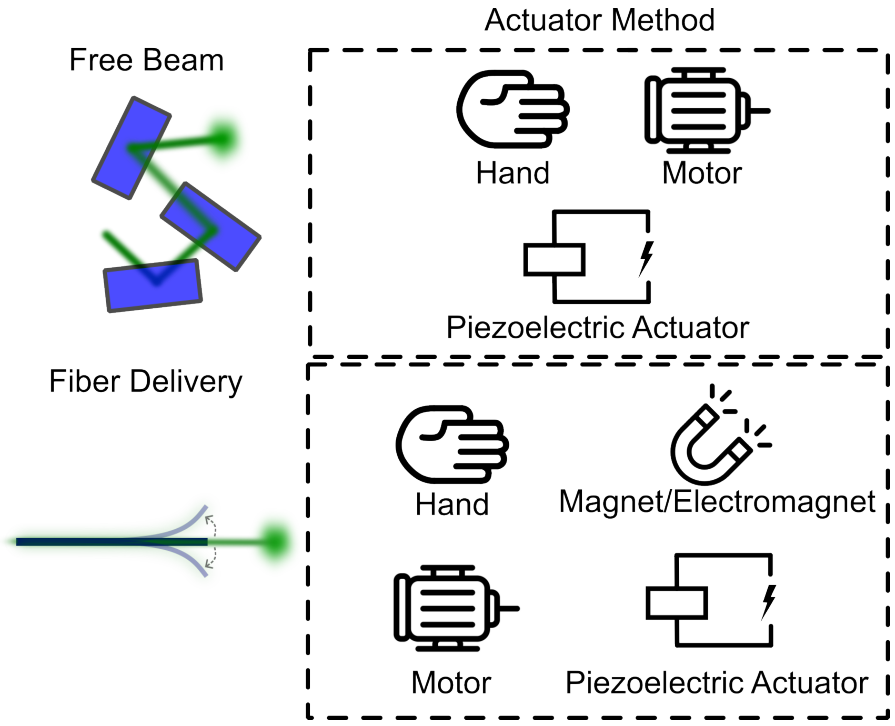

Figure 1.3: *Actuation methods for steering the beam of light.*

need for a direct line of sight because the beam is conveyed through flexible fibers [39, 40, 41, 42]. While these systems have proved their feasibility in gaining access to constrained surgical sites, the operation of these systems continues to be oriented toward use in the operating room. This prompts the consideration as to whether the concept of employing flexible instruments for laser-aiming tumors within the larynx can be transferred to office-based procedures.

Emerging as a new class of instruments, continuum manipulators offer dexterity within confined anatomical cavities [43]. These types of manipulators can adopt diverse curved configurations as shown in Fig. 1.4, distinguishing them from conventional manipulators by not relying on rigid links or joints, thereby facilitating their miniaturization [43]. Moreover, the utilization of continuum robotic manipulators aligns seamlessly with the capabilities of a flexible laser beam, providing adaptability to aim lesions within intricate anatomical spaces.

This work aims to enhance the effectiveness of surgical tools utilized in office-based laser procedures by introducing a new laser probe equipped with its own independent distal steering mechanism (Fig. 1.5). We hypothesize that providing physicians with an optical fiber equipped with additional degrees of freedom could significantly extend their reach within the laryngeal cavity. The proposed instrument in this dissertation is

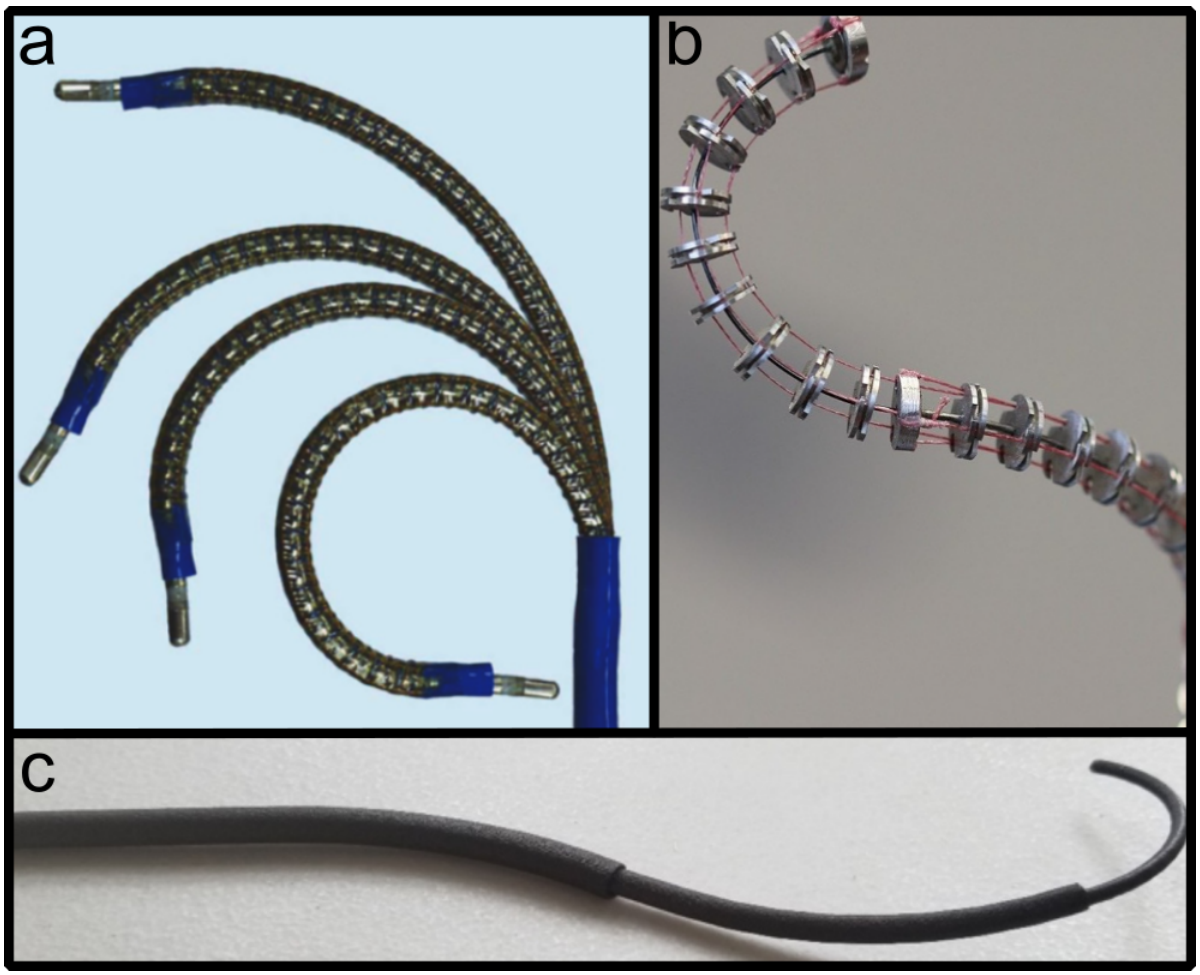

Figure 1.4: *Continuum manipulators: a) Hansen Medical Sensei system. A modern continuum robot used for medical applications. b) Tendon-driven continuum robot [44]. c) 3D-printed Concentric Tube Robot [45].*

a Steerable Optical Fiber (SOF) designed for deployment into the instrument channel of a laryngoscope providing independent articulation, and allowing precise targeting of lesions in the larynx. Shifting the paradigm of treatment towards more convenient and patient-friendly office settings not only could optimize the efficiency of healthcare delivery but also underscores a commitment to patient-centered care.

1.4 Scope of the thesis

This thesis establishes a comprehensive analysis, conceptualization, and implementation of a Steerable Optical Fiber (SOF) to thermally ablate diseased tissue placed in hard-to-reach locations within the larynx. The overarching goal is to enhance precision in

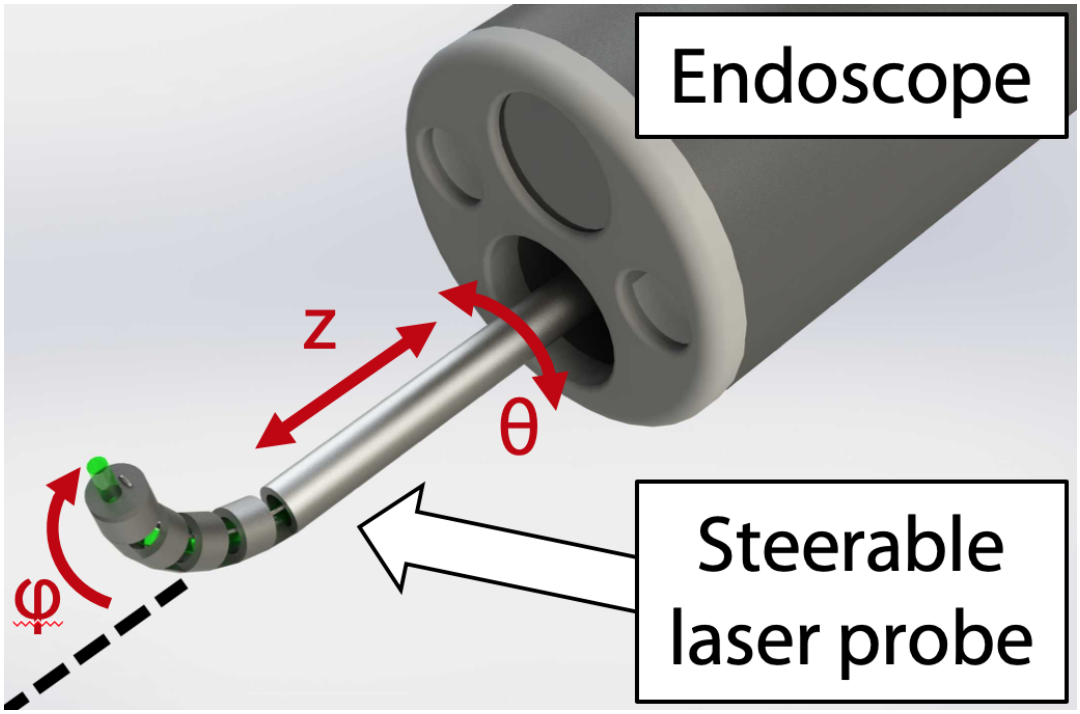

Figure 1.5: *Concept of the Steerable Optical Fiber.*

surgical laser-aiming and extend the reach to previously inaccessible regions within the laryngeal cavity. The main contributions of this dissertation are summarized as follows:

1. A simulation framework to identify all the inaccessible regions within the larynx anatomy in endoscopic laser surgeries. This simulation framework presents three-dimensional stereolithography (STL) models of the human larynx generated from a series of microtomography x-ray scans [46] and formulates the kinematic characterization of the endoscope following the methodology outlined in [47].

2. A Steerable Optical Fiber for laryngeal office procedure. This involves designing and modeling the steerable sheath using an asymmetric notch pattern recently proposed in the medical devices literature [20]. The new instrument provides three independent degrees of freedom (DoF), enabling precise aiming of lesions in hard-to-reach areas of the larynx.

3. A control mechanism designed for single-handed operation of the steerable fiber, ensuring minimal alteration to the existing clinical setting for in-office laser surgery. We demonstrate in a preliminary user study the feasibility of reaching effectively challenging surgical sites compared to traditional instrumentation.

1.5 Outline of the thesis

The remaining chapters of the thesis are organized in the following manner:

Chapter 2 describes the larynx anatomy, as well as the surgical management of certain medical conditions of the larynx. We also discuss existing technical approaches for laser aiming in these interventions.
Chapter 3 describes the simulation framework to characterize the inaccessible regions within the larynx, including the kinematic modeling of the current instrumentation.
Chapter 4 describes the design and modeling of the proposed Steerable Optical Fiber. We analyze the feasibility and effectiveness of the tool for treating lesions in the larynx.
Chapter 5 describes the design and validation of the single-handle controller to operate the steerable optical fiber.
Chapter 6 concludes the thesis and discusses future avenues of research, including further clinical validation, refinement of control mechanisms, and potential integration of advanced imaging techniques.

CHAPTER 2

EXPLORING THE LARYNX: ANATOMY, PATHOLOGIES, AND SURGICAL INTERVENTIONS

2.1 Larynx Anatomy

The larynx, commonly referred to as the voice box, is a complex anatomical structure located at the upper level of the airway [48]. The main functions of the larynx are voice production, protection of the airway during respiration, and swallowing. The larynx anatomy can be split into three distinct regions known as the *supraglottis*, *glottis*, and *subglottis* [49] (Fig. 2.1).

The supraglottis is the upper part of the larynx, situated above the glottis. It includes anatomical structures such as the laryngeal inlet, the laryngeal ventricle (the space between the false and true vocal folds), the false vocal folds, the posterior surface of the epiglottis, arytenoid cartilages, and medial aspects of the aryepiglottic folds [49, 50]. The false vocal folds, also known as vestibular folds, are a pair of thick folds covered by respiratory mucosa. The laryngeal ventricles are paired narrow air-filled spaces positioned between the true and false vocal cords. They extend laterally in a spindle-shaped manner, forming what is known as the laryngeal saccule. Assessing the complete extent of the laryngeal ventricle endoscopically can be challenging because of the narrow and recces location [48, 49, 50]

The glottis consists of the paired true vocal folds, the anterior and posterior commissures, and the rima glottidis between them [48]. The vocal folds are two bands of

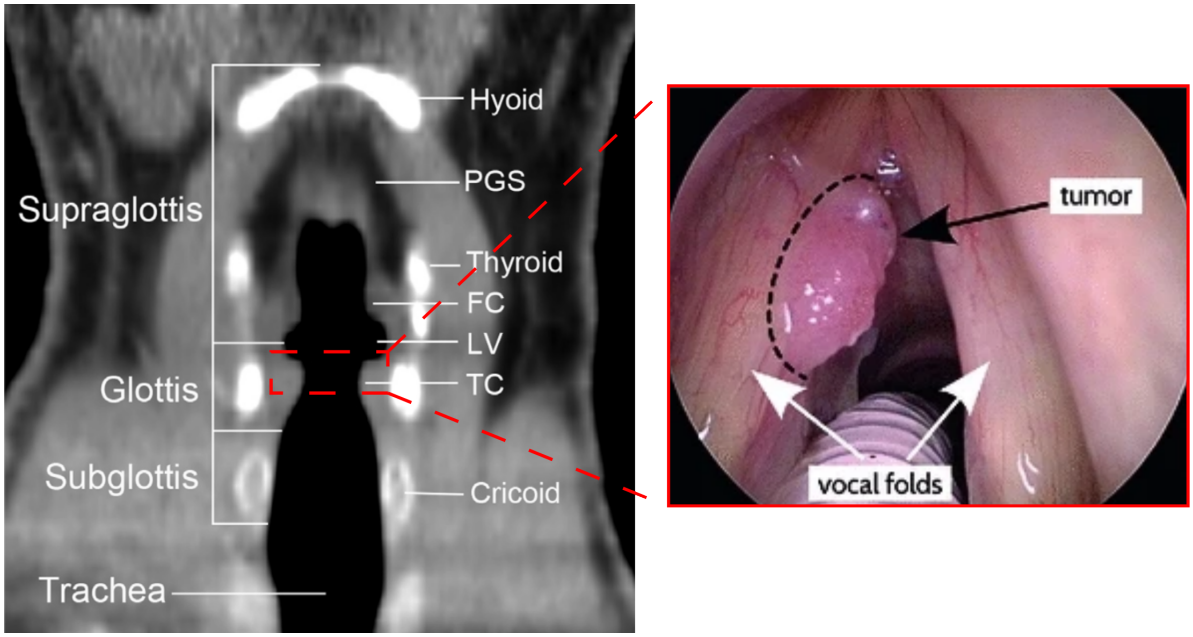

Figure 2.1: *Coronal CT image showing the regions of the human larynx [50]. Inset of the glottis region showing a squamous cell carcinoma affecting the vocal folds [51].*

smooth tissue positioned opposite each other within the larynx. The vocal folds comprise three main components: a muscle known as the vocal muscle or internal thyroarytenoid muscle, the vocal ligament, and a covering mucosa [52, 53, 54] as Fig. 2.2 illustrates. The vocal ligament forms the inner edge of the laryngeal triangular membrane. The ligament is part of the larger thyroarytenoid muscle and lies external to the laryngeal quadrangular membrane. This muscle forms the core of the vocal folds. The vocal muscle lies internally, adjacent to the laryngeal quadrangular membrane. Its fibers run parallel to the vocal ligament. The covering mucosa envelops both the vocal ligament and the vocal muscle. It is composed of a squamous stratified epithelium and a layer of loose connective tissue known as Reinke's space.

During periods of rest, the vocal folds remain open to facilitate breathing, while, when speaking, the vocal folds rapidly close as air from the lungs passes through, causing them to vibrate. These vibrations generate sound waves that propagate through the throat, nose, and mouth, acting as resonating cavities to modulate the sound [55].

The subglottis extends from 1 cm beneath the free edge of the vocal folds to the lower edge of the cricoid cartilage. Assessing the subglottis on imaging is typically straightforward because it consists of a thin layer of mucosa along the inner surface of the cricoid and tracheal cartilage [48, 50]

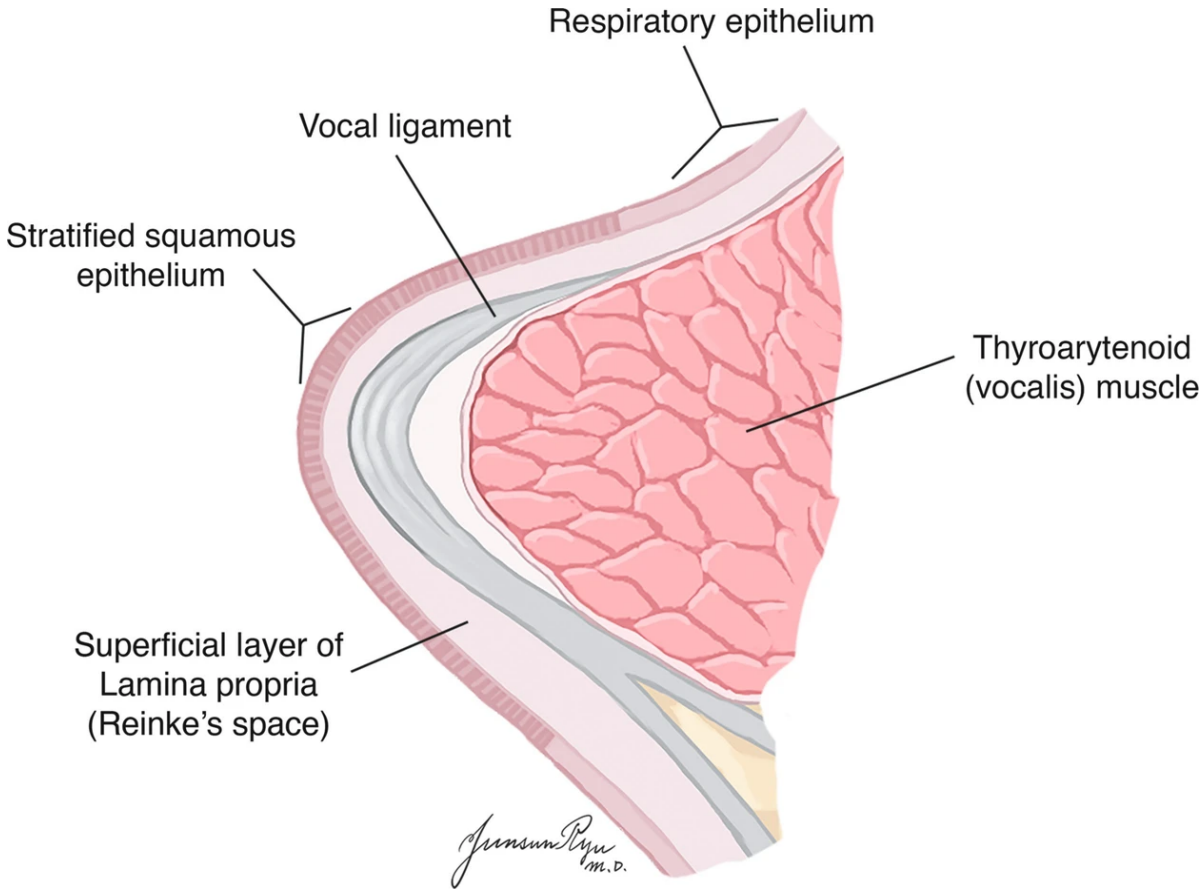

Figure 2.2: *Multilayer structure of the Vocal Fold [54].*

2.2 Laryngeal Disorders: Medical Conditions and Treatment Modalities

In this section, we provide an overview of the pathologies that may affect the laryngeal anatomy and the evolving treatment modalities utilized in clinical practice.

2.2.1 Medical Conditions

Abnormal growths can sometimes form on the vocal folds, impacting voice quality [3, 56]. Vocal nodules, for example, appear as swelling on both sides of the vocal folds. These lesions are commonly observed in children, adolescents, and predominantly female adults with vocally demanding professions [56]. In contrast, vocal polyps are usually found in men and typically are unilateral growths on the vocal folds. The factors attributed to their development are intense intermittent voice abuse, aspirin or anticoagulant use, and vocal trauma from endotracheal intubation [56]. Cysts, another type of vocal fold mass,

are forming as sacs filled with fluid or tissue within the vocal cords. They may arise as mucus retention cysts or epidermoid cysts, with mucus retention cysts forming due to obstruction of mucous gland ducts, often associated with upper respiratory infections or vocal overuse [56].

Squamous Cell Carcinoma (SCC), a prevalent form of laryngeal cancer, is among the most serious conditions affecting the vocal folds. SCC is a common type of throat cancer linked to smoking and drinking. It forms in the outer layers of throat skin cells and can spread to nearby structures leading to significant voice and breathing disorders [51]. Fig. 2.1 shows a magnified view of the human vocal folds, on which SCC is highlighted. Annually, between 11 000 to 13 000 people are diagnosed with laryngeal cancer. SCC represents 85% to 95% of cases, significantly contributing to the morbidity and mortality associated with laryngeal cancer globally [35].

2.2.2 Treatment Modalities

The medical conditions described earlier (nodules, polyps, and cysts) may require surgical intervention for effective treatment. Advanced procedures such as microsurgery or laser surgery aim to precisely remove or repair damaged tissue, thereby facilitating the restoration of optimal vocal function. In this section, we discuss the current procedures for the surgical management of laryngeal lesions.

2.2.2.1 Transoral Laser Microsurgery

Transoral Laser Microsurgery (TLM) is a minimally invasive technique used to treat conditions in the glottis and supraglottis regions of the throat. It involves the use of a surgical laser and specialized microsurgical techniques to precisely remove or treat lesions while minimizing damage to surrounding healthy tissue [57].

The procedure is typically performed using a laryngoscope, which provides the surgeon with adequate visualization and access to the surgical site. Fig. 2.3 illustrates how TLM works. A metallic straight tube is inserted through the patient's mouth enabling surgical access to the throat. The surgeon conducts the procedure through the laryngoscope, using a microscope, a laser micromanipulator, and long microsurgical forceps.

One of the challenges associated with TLM is the manual control of the laser beam from outside the patient's body, often at a significant distance (typically 400 mm) from the surgical site. The extensive operational distance results in precision and consistency challenges when aiming the laser. Additionally, the long-distance constraint imposes

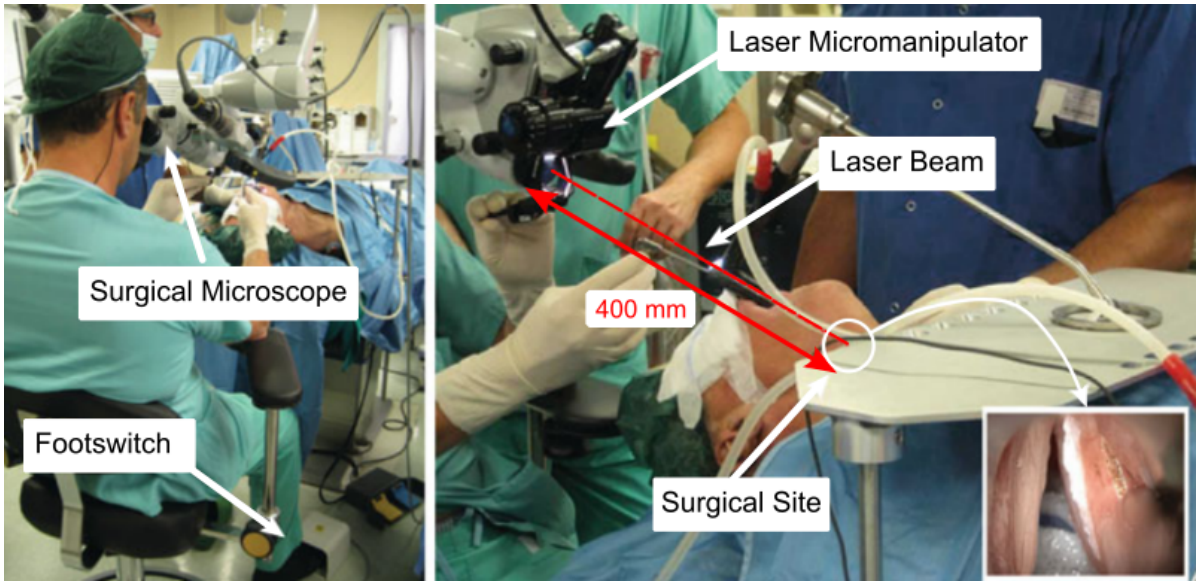

Figure 2.3: *Surgical configuration for transoral laser microsurgery. The surgeon controls the laser activation via the footswitch. The micromanipulator, shown at the right, enables precise control over the surgical site. The standard operating distance between the micromanipulator and the surgical field is* 400 mm *[51].*

a strict requirement for direct line-of-sight for controlling the laser [57]. Thus, certain patients are not eligible for TLM. Furthermore, the current configuration for TOLMS lacks of an ergonomic design, complicating the performance of high-precision surgical tasks. Surgeons require armrests to stabilize their hands while performing delicate maneuvers with the laser micromanipulator and long laryngeal forceps.

The European project μRALP, shown in Fig. 2.4, made significant progress towards addressing the obstacles encountered in TLM [57], particularly in overcoming constraints related to accessing the surgical site and establishing a direct line-of-sight for operations. To achieve this, the innovative concept of μRALP involved the development of teleoperated surgical system incorporating a micro-robot laser micromanipulator and a customized flexible endoscope. This setup enables the integration of advanced imaging and surgical technologies close to the surgical field, facilitating enhanced precision and effectiveness in minimally invasive procedures.

2.2.2.2 In-Office Laser Surgery

Office-based laser surgery is an emerging trend in Otolaryngology, where it is used to treat a variety of benign and pre-malignant tumors of the vocal folds [7, 11, 12]. These procedures are performed with the approach illustrated in Fig. 1.1: a laser fiber is

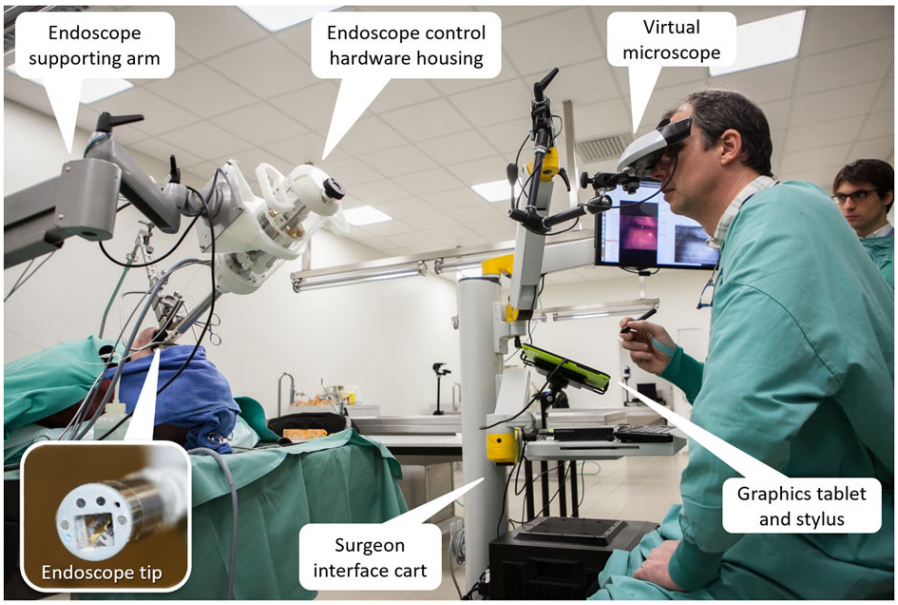

Figure 2.4: *Prototype of the integrated μRALP surgical system under evaluation in a human cadaver [57].*

deployed through the endoscope's operating channel to deliver laser pulses and thermally coagulate diseased tissue. This approach represents a paradigm shift from traditional tumor management strategies, which are normally based on surgical resection in the operating room. Prior studies have found office-based laryngeal procedures to enable considerable savings for patients [13, 14]. Furthermore, office procedures can be simply carried out under local anesthesia without sedation or using only a mild sedative [7, 12], therefore, enabling the treatment of ineligible patients to receive general anesthesia, e.g., elderly patients.

2.2.3 Laser Aiming Technology for Laryngeal Surgery

As we introduced in section 1.3, laser aiming systems for endoscopic surgery can be broadly classified into two distinct categories: free beam laser systems and fiber delivery systems (refer to Fig. 1.3). Here, we describe the details of these systems, elucidating their respective functionalities and applications within laryngeal surgery.

Table 2.1 provides an overview of the latest advancements in laser aiming systems as documented in the existing literature. These systems vary in size and functionality, with ongoing direction towards miniaturization to facilitate access and maneuverability to constrained anatomical environments such as the vocal folds. Despite significant advancements in size reduction and operational flexibility, their integration into office

Table 2.1: *Laser Aiming Systems*

Research Group	Laser System	Size [mm]	Laser Source
Acemoglu et al [39].	Fiber	13	625 nm laser
Kundrat et al [40].	Fiber	11.5	650 nm laser
Zhao et al [41].	Fiber	22	Thulium Laser
Fang et al [42].	Fiber	12	808 nm laser
Patel et al [58].	Free Beam	17	CO2 Laser
Rabenorosoa et al. [36]	Free Beam	8x10	-
Renevier et al [37].	Free Beam	9x11	Er:YAG
York et al [38].	Free Beam	18x18	-

settings remains an ongoing consideration.

2.2.3.1 Free Beam Laser Systems

In free beam systems, aiming is achieved through rapid displacements of a deflecting mirror [34]. Surgical laser devices utilizing this aiming method have been restricted by their large size, limiting their application in minimally invasive surgery. To address this constraint, research has been directed toward developing miniaturized free beam-based laser steering systems while maintaining comparable outcomes such as a laser steering speed higher than 1000mm s^{-1}.

Piezoelectric actuators have been employed for the control of mounted optical mirrors. The properties of piezoelectric actuators, such as their compact size, high precision, and rapid response, have facilitated the miniaturization of the laser steering system while ensuring without compromising positional accuracy and laser steering speed. Rabenorosoa et al [36] utilized a series of linear piezoelectric actuators to manipulate a laser beam for vocal fold surgery. They developed a compact system (18mm) with two degrees of freedom that entailed a pan-tilt mirror mechanism driven by linear piezoelectric motors to adjust the direction of the laser beam (Fig. 2.5 (h)). While this approach effectively reduces the size of the free beam laser steering system, it requires

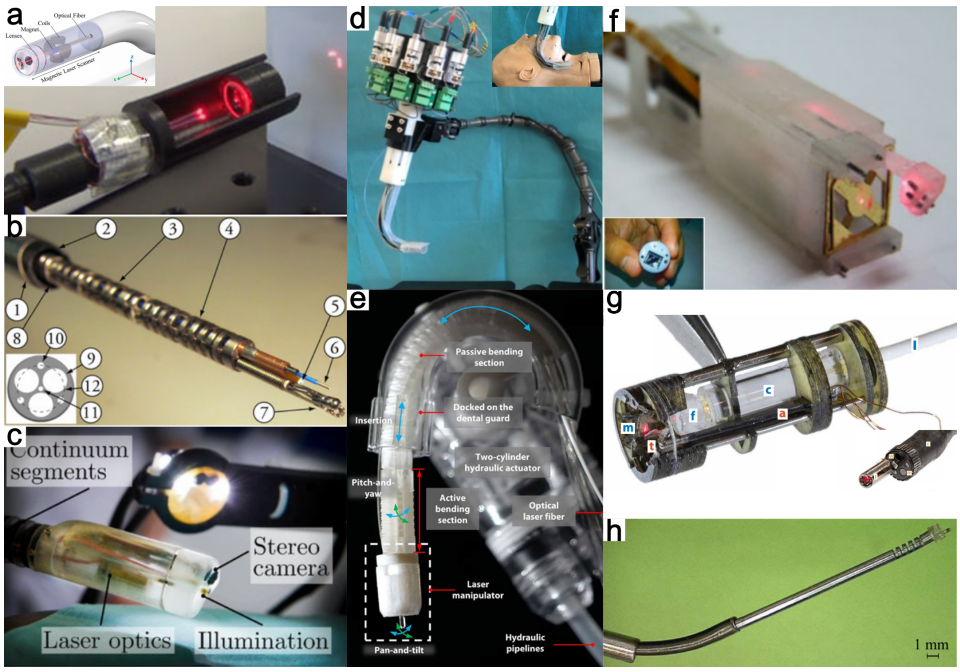

Figure 2.5: *Summarizes recent research on laser aiming systems in surgery. (a) Magnetic actuator-driven optical fiber steering robot [39]. (b) Backbone-based optical fiber steering robot [59]. (c) Motor-actuated push-pull rods for fiber steering robot [40]. (d) Motor-actuated with cables for fiber steering robot [41], (e) Hydraulic actuation for fiber steering robot [42]. (f) Piezoelectric actuator-driven free beam laser steering robot [36, 37]. (g) Piezoelectric actuator-driven for steering free beam laser [38]. (h) Hybrid concentric tube-based optical fiber steering robot [60].*

the use of a fixed external prism to direct the laser toward the mirror. Furthermore, the overall dimensions of the system depend on the commercially available piezoelectric actuators, which presented obstacles to achieving further size reduction.

York and colleagues [38] present an alternative mirror configuration for free beam laser steering (Fig. 2.5 (i)). They implemented a three-mirror design consisting of one fixed mirror and two movable mirrors. This configuration allows to maintain the focal distance of the laser even as the orientation mirrors change. Furthermore, the dimension of the system is significantly reduced to reach an overall size of 6mm. Finally, the system presented by York is one of the fastest systems documented in the literature, achieving a laser steering speed of 3900mm s^{-1}.

Recent research in free beam-based laser steering systems has led to notable improvements in their performance through the use of various types of piezoelectric actuators and transmission mechanisms. Despite these advancements, several technical challenges remain before these systems can be effectively utilized in clinical settings [34]. These

challenges include the need for further investigation and testing of suitable optical components capable of delivering high-power laser beams, considering the diverse requirements of different medical procedures. Additionally, it requires addressing electrical safety concerns associated with piezoelectric actuators, which typically operate at high voltages ranging from 0 to 200V. Finally, the actuators and transmission mechanism need to be fully enclosed to ensure their protection, durability, and sterilization for their successful integration into medical applications.

2.2.3.2 Fiber Laser Systems

Enhancing the flexibility, biocompatibility, and light transmission of optical fibers holds considerable promise in treating various clinical conditions, including those affecting the larynx [34]. Multiple research groups have focused on developing systems to integrate and control optical fibers, aiming to conduct surgeries accurately.

Acemoglu et al [39]. introduced a magnetic actuation system to steer the tip of an optical fiber in multiple directions for vocal fold surgery (Fig. 2.5 (e)). The design of their system includes attaching a permanent magnet ring to the optical fiber and incorporates four sets of miniature electromagnetic coils around the magnet. Despite the electromagnetic coils increasing the overall diameter of the system to approximately 10 mm and limiting the range of motion of the optical fiber within the system enclosure, the fiber could be manipulated with power as low as 1.5 W.

One of the limitations of magnetically actuated laser systems is that the electromagnetics coils introduces heating problems. As these electromagnets generate magnetic fields through current, they can produce heat within the system, presenting a challenge in effectively dissipating this heat without affecting the operating environment. Additionally, current efforts to miniaturize magnetic actuator-driven robots often involve off-board magnetic actuation, requiring a larger and stronger magnetic field generator due to increased distance. This can potentially disrupt the functionality of other medical instruments and metallic surgical tools. While placing the magnetic field generator closer to the system can mitigate this problem, it may not always be practical depending on the clinical scenario. Thus, future implementations of magnetic actuation for optical fiber steering must carefully balance the size systems with its performance requirements, considering factors such as range of motion and power needs.

An alternative method for laser aiming control involves continuum robots. These robots feature a flexible distal end, which is responsible for controlling the movement of an embedded optical fiber. Unlike traditional manipulators, continuum robots are a novel

class of manipulators capable of assuming potentially any curved shape and therefore they can be easily miniaturized [43]. We describe in detail continuum manipulators in section 2.3

Backbone-based manipulators are a common design among continuum robots, featuring an elastic structure with cavities for a working channel and actuation cables as shown in Fig. 2.5 (a). Goldman et al. [59] built from elastic materials such as Nitinol (NiTi) tubes, the manipulator bends in response to an applied force and returns to its initial position once the force is released. Actuation cables, routed through the cavities and anchored to the tip of the manipulator and motors, provide the necessary torque to bend the elastic structure effectively. These manipulators can be miniaturized to 5 mm and offer a range of motion exceeding the volume of a ϕ 40mm sphere. .

2.3 Modeling Continuum Manipulators

Continuum manipulators represent a novel category of actuators capable of adopting curvilinear shapes. In contrast to traditional hyper-redundant manipulators, continuum manipulators are not characterized by discrete links, which facilitates miniaturization [43]. In this section, we review the approach for modeling continuum manipulators.

In previous research, Webster et al. [47] established a comprehensive framework for modeling the kinematics of continuum robots. The fundamental assumption of this framework is that continuum robots bend in a manner described as a sequence of piecewise constant curvature segments. Each segment is characterized by a set of arc parameters, including arc curvature (κ), arc length (s) and rotation (ϕ), as illustrated in Fig. 2.6

To model the forward kinematics of continuum manipulators, we can decompose the process into two steps, as shown in Fig. 2.7, i.e., a robot-dependent mapping between the configuration space of the robot and the arc parameters, and the robot-independent mapping between the arc parameters and the task space. The robot-dependent mapping captures the relationship between actuator variables and the manipulator shape; As the name implies, such relationship are specific to each robot. The robot-independent mapping, instead, converts arc parameters into task space coordinates. Such mapping is purely geometrical, and its derivation does not depend on a specific actuation strategy. In the remainder of this section, we illustrate how to derive the robot-independent mapping for a continuum manipulator, under constant curvature assumptions. We will employ this model in both Chapters 3 and 4 of this thesis.

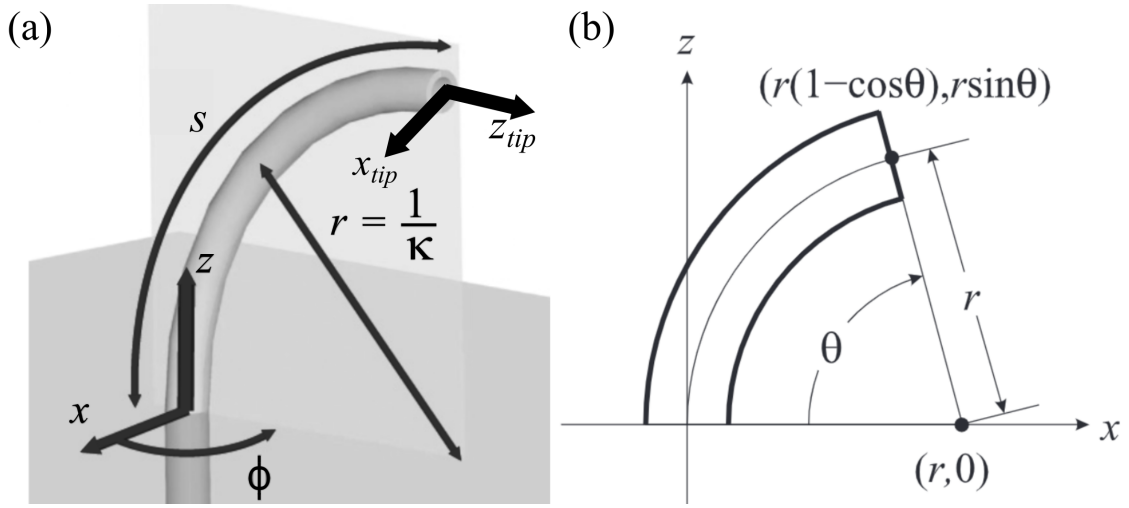

Figure 2.6: *a) The arc parameters represent a constant curvature segment: the curvature of the arc, κ, the base rotation, ϕ, and the arc length of the tube, s. b) When ϕ is zero, the arc lies in the x–z plane. Adapted from [47].*

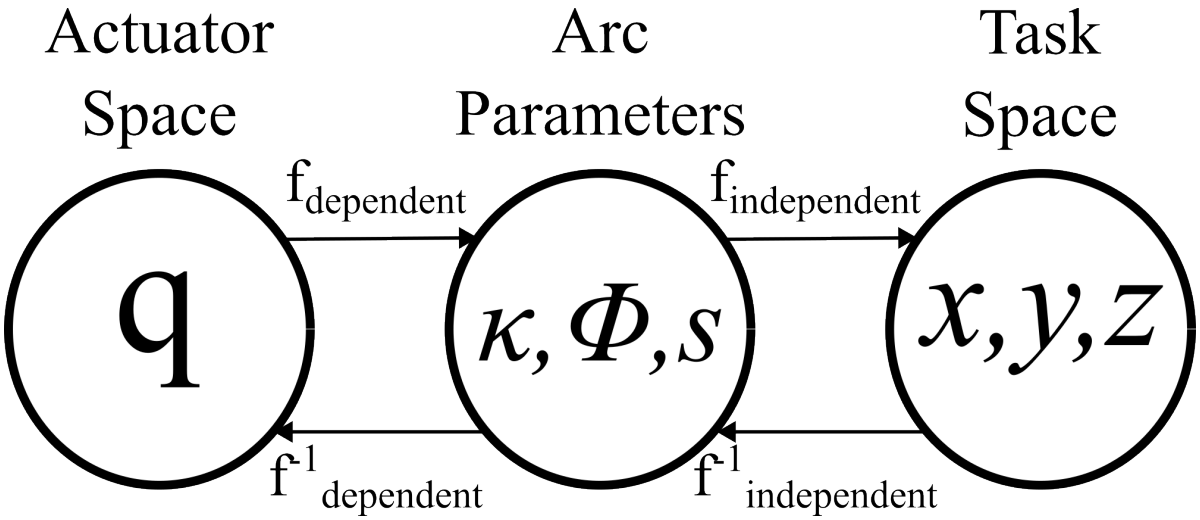

Figure 2.7: *To define the tip position of a continuum manipulator, the variables in the actuator space are mapped into a set of arc parameters, curvature (κ), rotation (ϕ), and arc length(s). Then, the arc parameters are mapped into the task space to determine the tip position of a continuum manipulator.*

The homogeneous transformation for a circular arc can be decomposed into two components: a rotation and an in-plane transformation.

$$T = e^{\hat{\xi}_{rot}\phi} e^{\hat{\xi}_{inp}s} \tag{2.1}$$

We can write the twist coordinates associated with each component as:

$$\xi_{rot} = \begin{bmatrix} v_{rot} \\ w_{rot} \end{bmatrix} = \begin{bmatrix} 0 & 0 & 0 & 0 & 0 & 1 \end{bmatrix}^T \tag{2.2}$$

$$\xi_{inp} = \begin{bmatrix} v_{inp} \\ w_{inp} \end{bmatrix} = \begin{bmatrix} 0 & 0 & 1 & 0 & \kappa & 0 \end{bmatrix}^T \tag{2.3}$$

where v and w are linear and angular differential motions respectively. The operator ^ maps twists from $\mathbb{R}^6$ to elements of $\mathfrak{se}(3)$, i.e. the Lie Algebra of the special Euclidean group SE(3) [61].

$$\hat{\xi}_{rot} = \begin{bmatrix} \hat{\omega}_{rot} & v_{rot} \\ 0 & 0 \end{bmatrix} = \begin{bmatrix} 0 & -1 & 0 & 0 \\ 1 & 0 & 0 & 0 \\ 0 & 0 & 0 & 0 \\ 0 & 0 & 0 & 0 \end{bmatrix} \tag{2.4}$$

$$\hat{\xi}_{inp} = \begin{bmatrix} \hat{\omega}_{inp} & v_{inp} \\ 0 & 0 \end{bmatrix} = \begin{bmatrix} 0 & 0 & \kappa & 0 \\ 0 & 0 & 0 & 0 \\ -\kappa & 0 & 0 & 1 \\ 0 & 0 & 0 & 0 \end{bmatrix} \tag{2.5}$$

Then, extending Eq. 2.1 we obtain:

$$T = \begin{bmatrix} \cos(\phi)\cos(\kappa s) & -\sin(\phi) & \cos(\phi)\sin(\kappa s) & \frac{\cos(\phi)(1-\cos(\kappa s))}{\kappa} \\ \sin(\phi)\cos(\kappa s) & \cos(\phi) & \sin(\phi)\sin(\kappa s) & \frac{\sin(\phi)(1-\cos(\kappa s))}{\kappa} \\ -\sin(\kappa s) & 0 & \cos(\kappa s) & \frac{\sin(\kappa s)}{\kappa} \\ 0 & 0 & 0 & 1 \end{bmatrix} \tag{2.6}$$

CHAPTER 3

CHARACTERIZATION OF LARYNGEAL OUTPATIENT ENDOSCOPIC LASER SURGERY

This chapter focuses on the identification of hard-to-reach locations within the larynx. Our objective is to develop a simulation framework to map the challenging areas that remain beyond the reach of conventional medical instruments. The overarching goal is to advance our understanding of laryngeal anatomy and subsequently enhance the operation of medical instrumentation during surgery by accurately mapping the challenging regions within the larynx.

For this purpose, we utilize microtomography X-rays [46] to create eight highly detailed three-dimensional larynx models. These models provide comprehensive representations of the anatomical structures within the larynx, laying the foundation for our subsequent efforts to identify and characterize hard-to-reach locations. Concurrently, we characterize the motion patterns of the endoscope utilized by physicians during laryngeal exploration.

Finally, we merge the larynx's detailed anatomical models with the endoscope's motion characteristics within a simulation framework (see Fig. 3.1). This framework enables us to analyze the functionality of the endoscope within the larynx, offering a meaningful understanding of the accessible surgical site. The simulation involves a sampling motion planning algorithm, specifically, the Rapidly-Exploring Random Tree (RRT) [62] to analyze and characterize the workspace of the current instrumentation and a ray-triangle intersection algorithm (Möller-Trumbore) [63] to delineate the operational

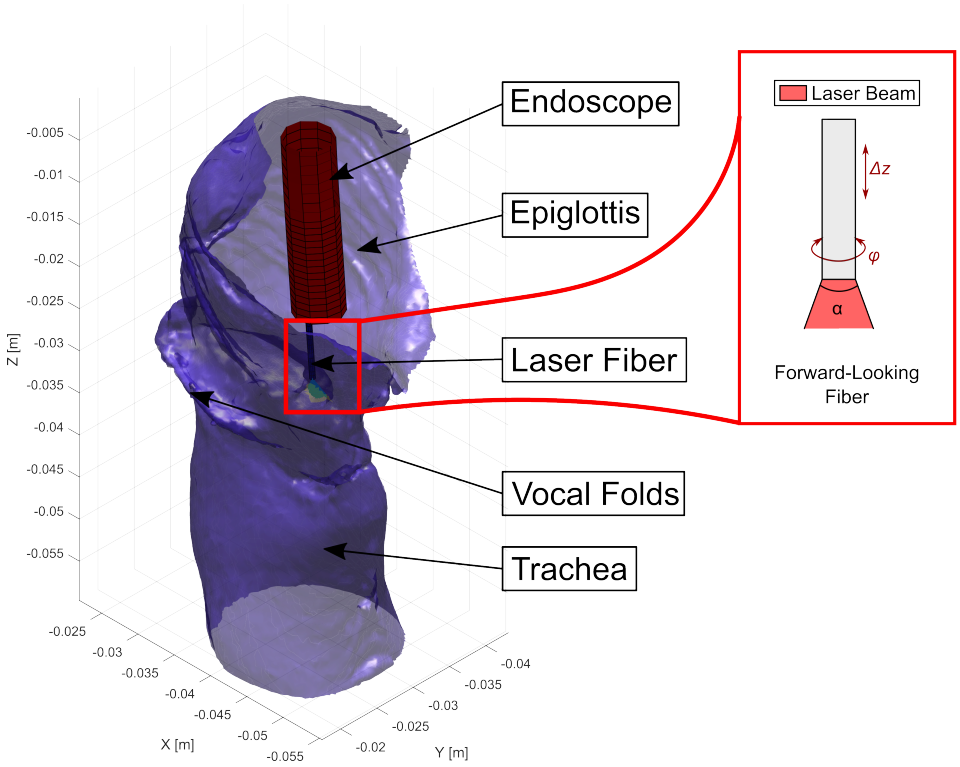

Figure 3.1: *Simulation Environment: an endoscope is deployed into a virtual larynx model and controlled by a sampling- based motion planning algorithm, i.e. Rapidly-Exploring Random Trees (RRT). The inset shows the forward-looking fiber that is currently used for laser surgery.*

map within the larynx. Through this systematic approach, we aim to advance our knowledge of the laryngeal anatomy and current medical tools.

3.1 Larynx Analysis

To analyze the laryngeal anatomy, we generated three-dimensional models of the larynx based on tomography images published by Bailly et al. [46] as Fig. 3.2 illustrates. These images were acquired with an X-ray microtomograph, with voxel sizes varying between 25 and 45 μm. Microtomography (μCT) X-ray scans offer enhanced resolution compared to standard computer tomography (CT) scans, allowing adjust the voxel sizes to twice to ten times smaller dimensions. This detailed resolution is particularly beneficial for capturing the structure of the vocal folds, which typically measure between 1.5 to 2 cm. Thus, μCT scans provide a more accurate representation of the vocal fold anatomy.

We initially processed the μCT to create the three-dimensional models using a custom

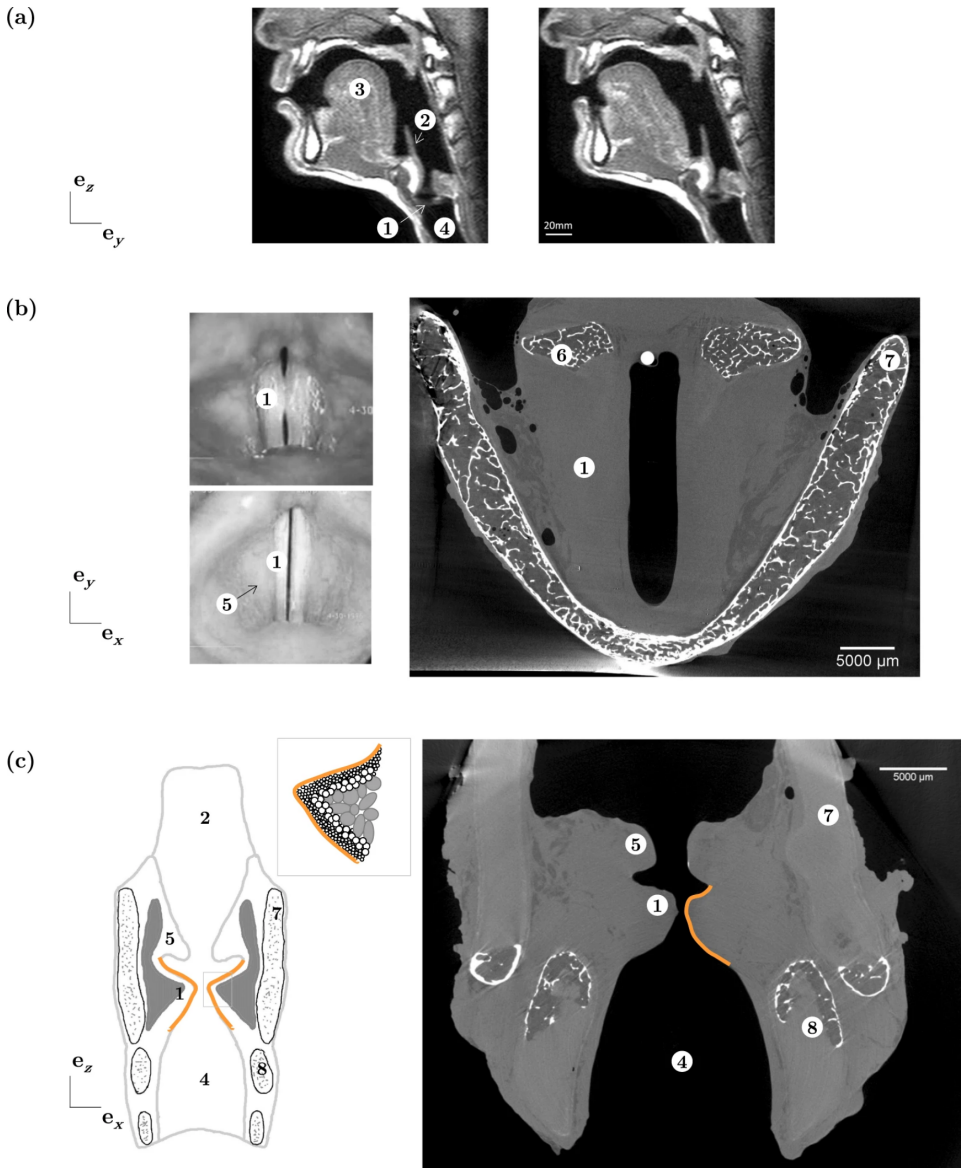

Figure 3.2: *Different imaging modalities are used to illustrate the human vocal system. (a) MRI images in the mid-sagittal plane capture the upper airways during the production of the sounds [u] and [e] by a male subject, sourced from GIPSA-lab. (b) A cross-sectional view of the vocal folds: on the left, in vivo video laryngoscopic footage captured during variations in sound pitch by a male subject; on the right, an ex vivo X-ray microtomographic image with a voxel volume of* $V_{vox} = 25^3\ \mu m^3$. *(c) Mid-coronal view of the larynx: (left) idealized scheme and zoom on the vocal-fold fibrous microstructure; (right) ex vivo X-ray tomographic image (L3,* $V_{vox} = 25^3\ \mu m^3$*). ① Vocal fold, ② Epiglottis, ③ Tongue, ④ Trachea, ⑤ Ventricular fold, ⑥ Arytenoid cartilage, ⑦ Thyroid cartilage, ⑧ Cricoid cartilage. Reproduced from [46].*

MATLAB script. This script facilitates the creation of three-dimensional stereolithography (STL) models, ensuring an accurate representation of the laryngeal anatomy captured in the scans. Then, we post-processed the STL models using the Quadric Edge Collapse Decimation filter in Meshlab [64]. This step aimed to decrease the number of vertices in the models to reduce the computational cost required for subsequent simulations and analyses.

To ensure comprehensive coverage of the anatomical variability, we generated eight larynx models from the data set. Each model was constructed to represent a range of anatomical variations observed within the dataset. By incorporating multiple models, we aimed to account for the inherent diversity in laryngeal structures among individuals.

3.2 Endoscope Analysis

To comprehensively map out the surgical access within the larynx, we studied the motion pattern of the endoscope. We hypothesize that the limitations in surgical access are closely related to the motion of the endoscope. Therefore, we aim to characterize the kinematics of the endoscope.

The endoscope utilized in our study is the Pentax VNL-1570STK14 [65] as shown in Fig. 3.3. The endoscope is a trans-nasal flexible laryngoscope with a diameter of 4.9 mm and a working channel of 2 mm. It is capable of axial translation, rotation, and in-plane bending, which define the 3 degrees of freedom (DoF) of the endoscope. In its standard configuration, the endoscope is inserted into the larynx with the chip-tip camera positioned above the right vocal fold, while the laser fiber is directed towards the left vocal fold as Fig. 1.2 (a) illustrates.

To model the motion of the endoscope, we assume that the bending occurs in the shape of a constant curvature arc as is shown in Fig. 3.3 b. Then, we use a well-known kinematics relation from the robotics literature [47]. The operational range of the endoscope was determined based on the insights of our clinical collaborator, a trained laryngeal surgeon. Therefore, in the simulation, the endoscope's bending ranges from -120° to 120°, while axial rotation is constrained within the interval of -100° to 100°.

3.3 Surgical Access Estimation

The configuration illustrated in Fig. 3.1 provides a detailed view of the simulation environment. A virtual flexible endoscope equipped with a laser fiber is deployed into

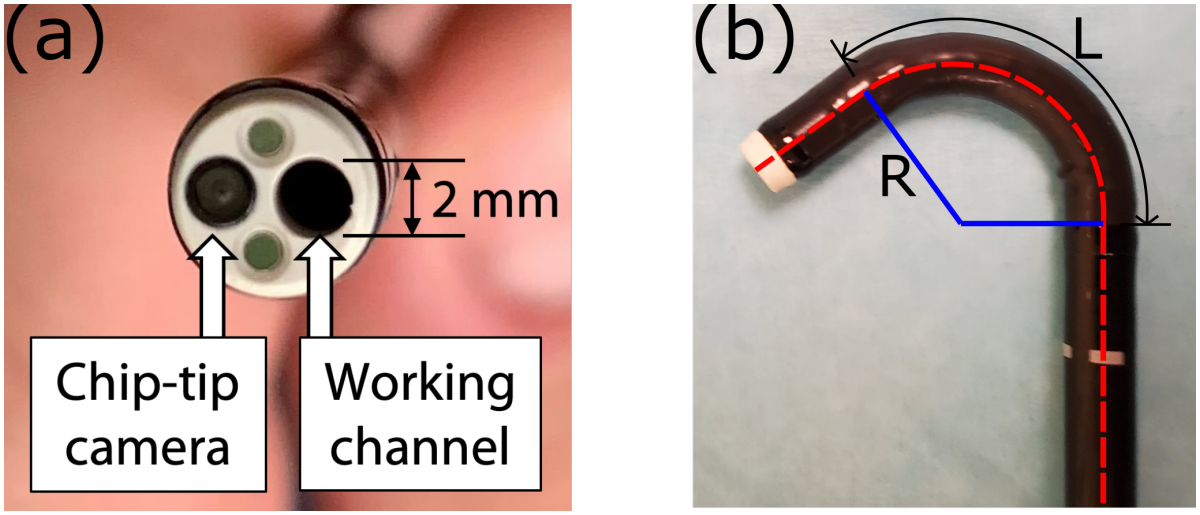

Figure 3.3: *Pentax VNL-1570STK video laryngoscope: (a) This flexible endoscope includes a chip-tip camera and a 2 mm side working channel; (b) View of the endoscope showing constant-curvature bending, with R being the (variable) bending radius and L = 25.7 mm being the length of the bending section.*

a three-dimensional model of the larynx. Then, a computer program controls the endoscope to explore the anatomy of the laryngeal cavity. This exploration is conducted systematically to cover the reachable areas within the larynx.

To characterize the reachable anatomy, we enable the endoscope to navigate through the laryngeal cavity utilizing a sampling motion planning algorithm, namely Rapidly-Exploring Random Tree (RRT) [62], to generate the workspace of the endoscope within the laryngeal cavity. This process involves sampling various configurations of the endoscope and determining feasible paths through the anatomical structures.

Once the reachable anatomy is characterized, we use the Möller-Trumbore ray-triangle intersection algorithm [63] to simulate the application of laser pulses over the surgical site. The Möller-Trumbore algorithm is commonly used for ray tracing in computer graphics to determine whether a ray intersects with a triangle in a three-dimensional space. Thus, we can determine the areas within the larynx that can be effectively treated with the laser pulses.

3.3.1 Reachable Workspace Characterization

To create a comprehensive map of the reachable tissue within the laryngeal cavity, we employ a sampling-based motion planning algorithm known as Rapidly-Exploring Random Trees (RRT) [62]. We generate ten thousand potential endoscope configurations,

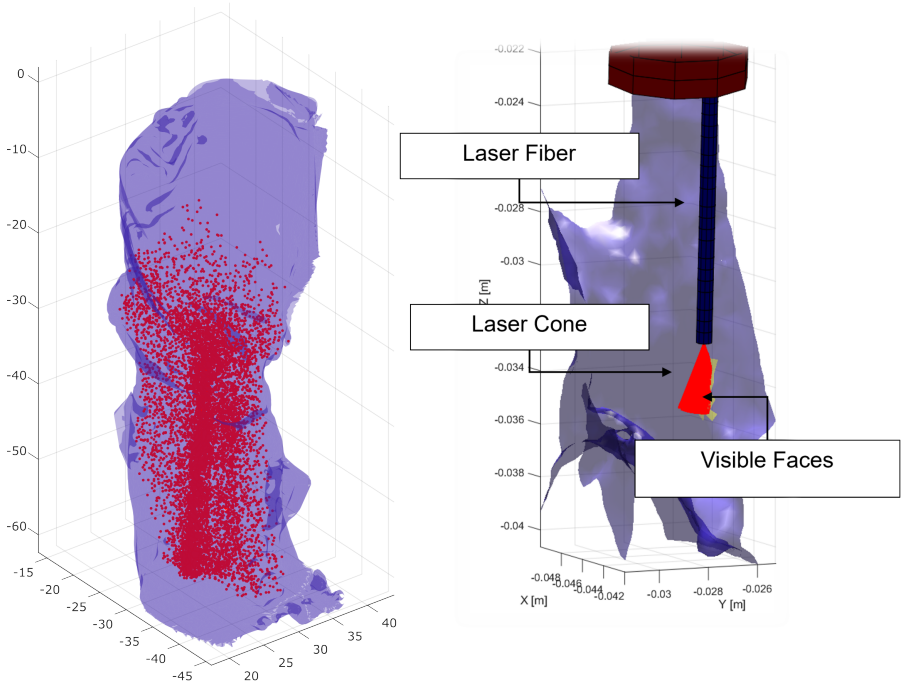

Figure 3.4: *(a) The reachable workspace within the larynx highlighted by red dots. (b) A simulation demonstrating the emission of light in a conical pattern from the tip of the laser fiber. When the light intersects with a triangle in the mesh causes the mesh to change color to yellow, indicating that it is a surgical site accessible by the laser fiber.*

along with the corresponding points indicating the tip position. Initially, we define the Degrees of Freedom (DoF) for both the endoscope and the laser fiber. The endoscope is characterized by three DoF: translation, rotation, and tip bending, while the laser fiber provides two DoF: translation and rotation. This results in a 5-dimensional vector, representing the configuration space of the endoscope system. Then, using the configuration space of the endoscope system, along with a forward kinematic model of the endoscope, we simulate the motion of the endoscope within the laryngeal cavity.

To utilize RRT for mapping the accessible tissue within the larynx offers several advantages. Unlike conventional motion planning techniques focused on point-to-point navigation, RRT enables systematic workspace exploration without being constrained to a specific destination. Thus, we can build the map of the reachable workspace represented by the red dots in Fig. 3.4 (a). Previous research, such as the one conducted by Alterovizt et al. [66] on characterizing the reachable workspace of a continuum manipulator in the lungs, underscores the effectiveness of this approach. Because RRT provides probabilistic completeness, the longer the algorithm is executed, it can guarantee the discovery of the entire reachable workspace.

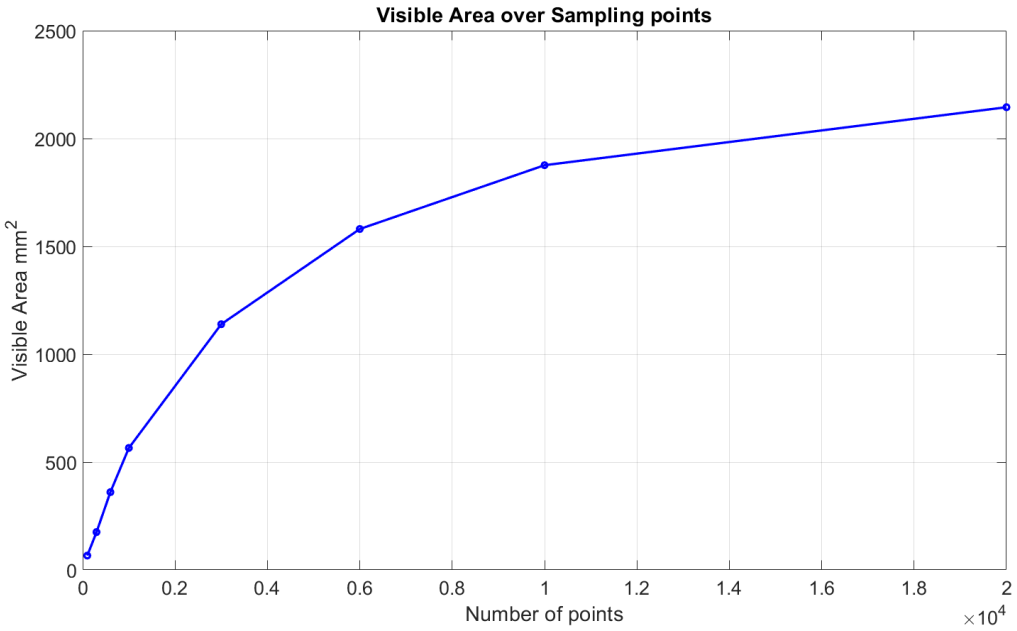

Figure 3.5: *Estimation of the visible area within the larynx relative to the number of sampling points. As the simulation advances, the curve representing this relationship gradually flattens, approaching an asymptote, indicating the revelation of the true extent of the workspace within the larynx.*

To determine the appropriate running time to ensure complete coverage of the reachable workspace, we rely on the RRT probabilistic completeness property. Every time we execute the algorithm, we consistently generate the graphic shown in Fig. 3.5. This graphic illustrates the relationship between the number of sampling points and the extent of the discovered workspace. As the simulation progresses, the curve illustrating this relationship gradually flattens, approaching an asymptote, meaning that we discover the true extent of the workspace. Thus, we monitor the growth rate of the curve and terminate the process when it reaches a plateau.

3.3.2 Laser Range Estimation

To identify the areas that can be effectively treated within the larynx, we simulate the application of laser pulses over the STL model of the larynx. Through each configuration of the endoscope, previously generated using the RRT algorithm, we employ a ray-casting algorithm to emulate the application of laser light. We generate 1,000 virtual rays from the fiber tip in a cone shape that mimics the dispersion pattern of the laser beam as Fig. 3.4 (b) illustrates.

Subsequently, from each of the virtual rays that form the conical laser beam, we use the Möller–Trumbore ray-triangle intersection algorithm [63] to detect which faces of the STL larynx model fall within the direct line of sight of the simulated laser pulses. A key to identify the treatable areas is assessing the proximity of the STL faces to the tip of the laser fiber. STL faces located more than 3 mm away from the fiber tip are identified as inaccessible for treatment because they would not be irradiated with a sufficient power density due to the divergence of the laser beam [67, 68]. On the other hand, each instance where the optical fiber effectively reaches a face of the STL model, that face is marked in yellow as Fig. 3.4 (b) shows. Furthermore, we ensure that the region receiving laser light remains visible to the endoscope camera by employing the ray casting algorithm once more, this time from the tip of the endoscope.

3.4 Simulations Results

The simulation results of larynx one and two are shown in Fig. 3.6. Among the eight larynx models used in the simulations, these two models are based on the anatomy of two deceased individuals who donated their bodies for research purposes [46]. Larynx 1 reproduces the anatomy of an 86-year-old female, while Larynx 2 is a 94-year-old male. Simulation results indicate difficulty accessing the cavity immediately above the vocal folds, as well as, we observed challenges in reaching the area below the vocal folds.

Further analysis of the simulation output revealed an interesting result, namely the presence of a well-defined gap in the point clouds representing the set of spatial locations reached by the tip of the laser fibers (see Fig. 3.7). This gap was observed in all the simulations, and it was always located on the right side of the larynx. After reviewing the simulation code to exclude the presence of programming errors, the finding was discussed with the clinical expert on our team, who confirmed that the right side of the larynx is, in fact, more challenging to access during an in-office procedure than the left side. When using a forward-looking fiber, the gap in the reachable volume causes a region on the right side of the larynx to become inaccessible. This issue has been previously reported in the medical literature [17], and it is attributed to how channeled video laryngoscopes are designed and operated. As it was shown earlier in section 3.2, the standard orientation for a laryngoscope is such that the chip-tip camera is positioned on the right side of the patient, while the laser fiber is on the left side (refer to Fig. 1.2 (a)).To aim the laser fiber on the right vocal fold, the endoscope could in principle be axially rotated by 180°. In practice, such a maneuver is rarely performed, as it would

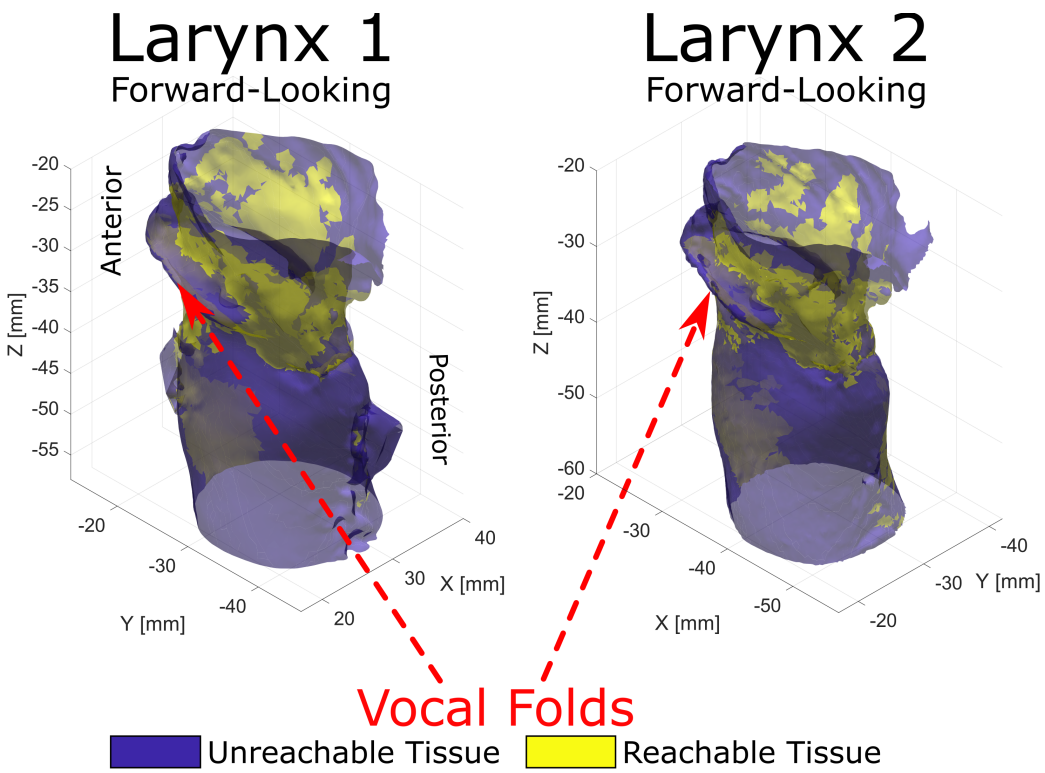

Figure 3.6: *Estimation of the reachable tissue in two different larynx models. Yellow surfaces mark areas that were found to be reachable by the traditional forward-looking laser fiber.*

require the operating physician to (1) flip the endoscope handle and hold it upside-down, and also (2) work with an inverted view of the anatomy. Both these things would make the procedure counter-intuitive to perform.

One of the limitations of the present study is that it does not account for the physiological motion that may occur during an office-based procedure. As noted earlier, office-based surgery is often carried out in awake patients, and the shape of the larynx may undergo alterations due to breathing or speaking. The STL models used to represent the shape of the larynx in this study are static objects, and they are thus not suitable to capture such shape changes.

Our results show that currently available instruments for office-based surgery have significant kinematic limitations (i.e., the workspace gap illustrated in Fig. 3.7), which, among other things, make it difficult to reach and treat lesions that develop on the right side of the larynx. These limitations were well-known in the clinical world [17] but they had not been quantitatively elucidated in the engineering literature yet. The results of our study help to fill this knowledge gap between clinical laryngoscopy and engineering,

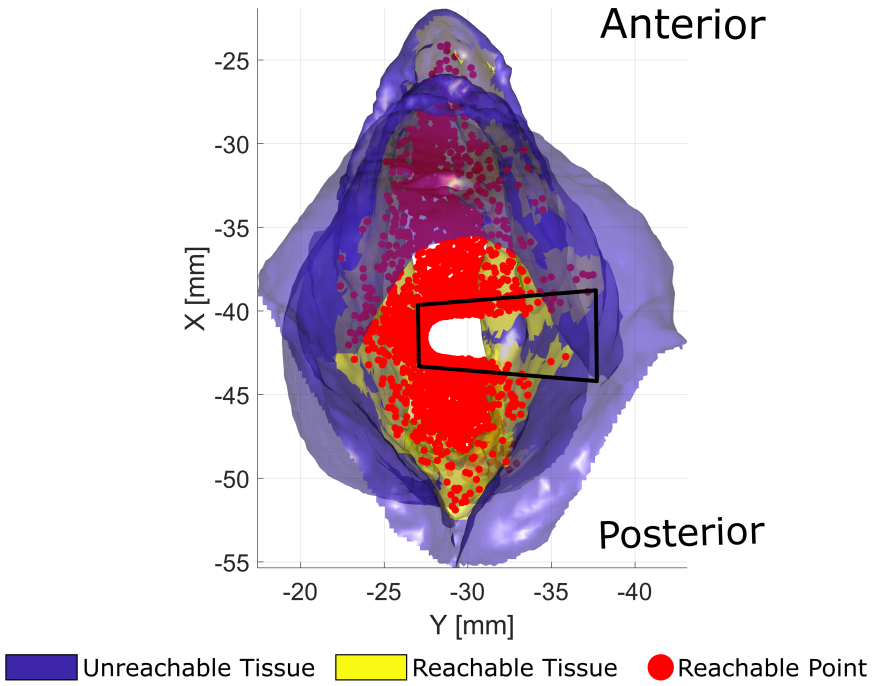

Figure 3.7: *Top view of Larynx 2, presenting the points reached by the forward-looking fiber in simulation. Across all simulations, we observed the presence of a gap in the point clouds, extending towards the right side of the larynx. These gaps suggest the presence of an inaccessible region within the larynx volume, consistent with observations previously documented in clinical literature [17]. For traditional forward-looking fibers, this inaccessible region causes an entire segment of the larynx impossible to access and treat.*

and they provide quantitative evidence that can be used in the future to guide the design of new laser fiber types for office-based vocal fold procedures.

CHAPTER 4

Steerable Systems for Endoscopic Laser Surgery of the Larynx

As we described in chapter 2, the endoscope employed for office-based laryngeal procedures needs to be sufficiently small to pass through one of the nostrils, and ideally as small as possible to minimize patient discomfort. The typical endoscope diameter for these procedures is 5 mm [12, 17]. Endoscopes are equipped with a working channel, typically 2 mm in diameter, which enables the passage of optical fibers for laser delivery. The overarching goal of laser surgery is to thermally destroy diseased tissue (e.g., cysts and nodules) via the application of laser pulses.

While office procedures are generally safe and effective, in section 3.4 we revealed that there exist several hard-to-reach locations inside the larynx where laser treatment cannot be delivered [16, 17]. This issue can be attributed to the limited dexterity of clinical instruments: the laser fibers used in-office procedures can only emit light forward in a line-of-sight fashion, making it hard to reach tumors that lie off the longitudinal axis of the fiber (refer to Fig. 1.2). Physicians can control the laser aiming by bending the distal tip of the endoscope; however, this does not provide sufficient anatomical coverage.

Given the outlined limitations, in this chapter, we focus on developing a methodology to overcome the maneuverability limitations inherent in current surgical tools. This involves designing, constructing, and validating a new steerable mechanism to enable optical fiber bending during endoscopic office procedures. The device, shown in Fig. 4.1 (b), is built by installing an off-the-shelf optical fiber into a tendon-actuated Nickel-Titanium (Nitinol) continuum notched sheath. The sheath diameter is 1.1 mm, which makes it

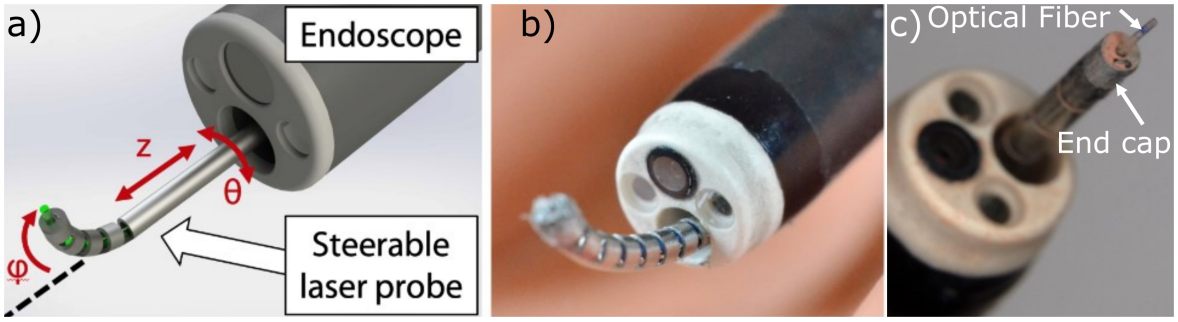

Figure 4.1: *a) Schematic of the proposed Steerable Optical Fiber. b)* 1.1 mm *Steerable Optical Fiber Prototype. c) Press-fitted end cap to house the optical fiber and the tendon-wire.*

suitable for trans-luminal deployment through the operating channel of most clinical endoscopes. We hypothesize that by providing surgeons with a steerable mechanism with additional Degrees of Freedom (DoF), we can increase the reachable area inside the larynx, thereby enhancing procedural precision and efficacy.

To assess the feasibility of the proposed approach, we initially simulate the operation of the steerable mechanism within the larynx. Our goal is to understand the potential capabilities and limitations of the proposed tool. Subsequently, we report experimental evidence, obtained in phantom experiments, documenting the ability of our device to navigate, reach and deliver laser pulses to regions within the larynx that are currently inaccessible in-office procedures.

4.1 Steerable Manipulator

To overcome the kinematic limitations of current clinical instruments, and thus amplify a physician's reach into the larynx, we propose to fabricate a steerable laser probe that can be deployed to the endoscope's instrument channel and independently articulated to aim target lesions in the larynx. Therefore, our steering mechanism enables control bending of the optical fibers used for laser delivery.

Several other groups are actively developing systems for laryngeal laser surgery [37, 39, 41, 40, 42, 57, 69] but none of the existing prototypes can be readily used in-office procedures. Thus, we formulated the specifications that guide our design process.

4.1.1 Design Specifications

4.1.1.1 Tool Miniaturization

The steering mechanism should be sufficiently small to permit the deployment of the fiber through the working channel of the operating endoscope, typically 2 mm in diameter. Meeting this specification is important to minimize patient discomfort: a larger mechanism would have to be deployed separately from the endoscope, either through the mouth or the other nostril. While several miniaturized laser steering mechanisms have been proposed in recent years [38, 70], none of them is sufficiently small to pass through the 2 mm lumen of a laryngeal scope.

4.1.1.2 Bending Radius of the Optical Fiber

The optical fiber utilized in our setup is the FP200ERT, sourced from Thorlabs (Newton, NJ, USA). This multimode fiber with a diameter of 0.225 mm is engineered to withstand bending radii as tight as 6 mm [71]. Exceeding this threshold could compromise the integrity of the fiber, potentially leading to failure to irradiate the appropriate power density. Therefore, ensuring the operation of the fiber within the specified bending range is fundamental to preserving the functionality and reliability of the optical fiber throughout our study.

4.1.1.3 Endoscope Field of View

We have to ensure that the tissue requiring laser treatment remains within the visual range of the endoscope camera. Administering laser treatment to a surgical site that lacks visualization from the camera would be impractical in the surgical setting. Thus, we verify the presence of a direct line-of-sight between the endoscope's lens and the target tissue. The Pentax endoscope provides a field of view of 85° [65].

4.1.2 Design Analysis

Given the outlined design specifications, we introduce the design of the steerable manipulator. Our objective is to create a steerable tool that maximizes the reachability inside the larynx. A schematic of the steerable manipulator, illustrating its components and dimensions, is shown in Fig. 4.2. It consists of an off-the-shelf optical fiber (FP200ERT) installed into a tendon-actuated Nitinol notched continuum sheath. For our prototype, we used a Nitinol tube with an outer diameter of 1.1 mm and a wall thickness of 0.1

Table 4.1: *Design Parameters of the Notched Sheath*

Name	Symbol	Value [mm]
Notch Width	w	0.94
Notch Spacing	u	1.31
Notch Height	h	0.19

mm. The distal end of the Nitinol sheath is outfitted with an aluminum end cap, which is installed by press-fitting. The end cap has three holes (Fig. 4.1 (c)): the center one, 0.3 mm in diameter, holds the optical fiber, while the other two, 0.2 mm in diameter, are used as attachment points for the actuation tendon. Fabrication of the end cap was carried out with a Super Mini Mill CNC machine (Haas Automation, Oxnard, CA, USA).

The steerable sheath uses the asymmetric notch pattern proposed by Swaney and colleagues in [20]. First, we establish the geometrical design parameters that define each notch represented in a 4-dimensional vector $d = [w\ h\ n\ u]$, where w is the width of the notches, h is the height of the notches, n is the total number of notches, and u represents the spacing between consecutive notches. The notch dimensions are illustrated in Fig. 4.2 and their values are listed in Table 4.1. In the following paragraph, we elaborate on the considerations regarding the selection of the design parameters.

The choice of the notch width w determines the amount of tendon pulling force necessary to bend the instrument: intuitively, the wider the notches are, the more compliant the steering section will be, and the less actuation force will be required to bend the endoscope. A full statics analysis for the bending mechanism is available in [20, 72, 73]. Another aspect to consider for the selection of w is the amount of strain that the remaining material in the notches will be subject to during bending: such a value should not exceed the maximum recoverable strain of Nitinol (which is typically quoted around 8%), otherwise, plastic deformation will occur. Typical values for w range between $80-90\%$ of the tube's outer diameter [20, 72, 73] as this has been proven to provide an optimal balance between stiffness and the force necessary for actuation.

Two important characteristics that capture the steerable manipulator's ability to reach distant locations and articulate around corners are the maximum bending angle θ_{max} and the steerable section length L shown in Fig. 4.2. From simple geometry, θ_{max}

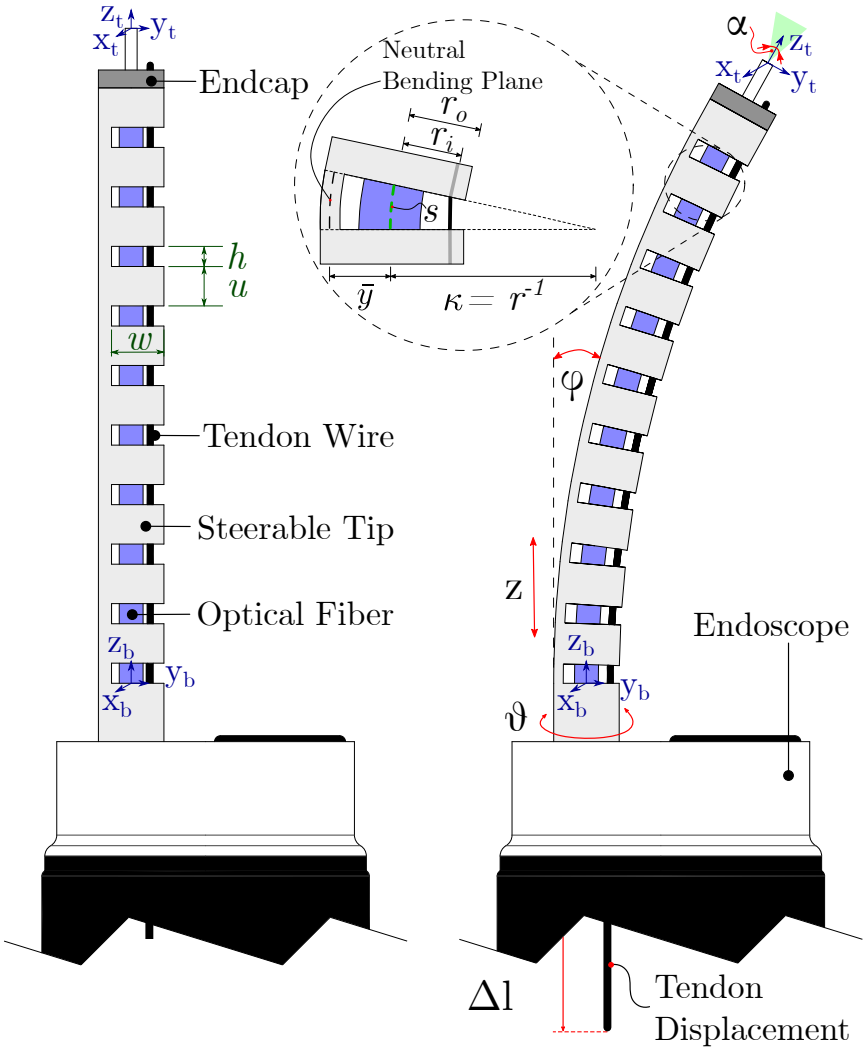

Figure 4.2: *The steerable manipulator consists of an optical fiber installed inside a tendon-actuated Nickel-Titanium (Nitinol) notched sheath. The actuation tendon is attached to an aluminum end cap installed at the distal tip of the sheath. Applying tension on the tendon makes the notches close, creating bending. When tension is removed, the sheath recovers its original undistorted configuration. (Left) Home configuration (no tension on the tendon); the design parameters of the notched sheath are the notch height h, the notch width w, and the spacing u between each pair of notches. (Right) The steerable manipulator provides three DoFs, namely tendon displacement Δl, axial translation z, and axial rotation ϑ. Each notch is assumed to bend in the shape of constant curvature arc, as per [20]. The laser beam divergence is $\alpha = 40°$. The inset shows the arc parameters that describe the deflection of a single notch, the arc curvature κ and the arc length s. Variables r_i and r_o indicate the inner and outer sheath radius, respectively.*

and L can be calculated as

$$\theta_{max} = n\frac{h}{r_o + \bar{y}} \tag{4.1}$$

$$Ł = n(h+u). \tag{4.2}$$

From Eq. 4.1 and Eq. 4.2, the number of notches (n), notch height (h), and spacing (u) all influence the maximum attainable bending angle θ_{max} and the length of the steerable section L. If we impose a desired maximum bending angle θ_{max}, we can derive a formulation for the notch height h:

$$h = \theta_{max}\frac{(r_o + \bar{y})}{n} \tag{4.3}$$

Similarly, if we impose a given length L of the steerable manipulator we can solve Eq. 4.1 for u:

$$u = \frac{L}{n} - h \tag{4.4}$$

The equations 4.3 and 4.4 still present a free parameter, i.e. the number of notches n. With θ_{max} and L now constrained, this parameter becomes a measure of how closely the tool bends in the shape of a constant curvature arc.

4.1.3 Kinematics Modeling

Our steerable manipulator is equipped with three degrees of freedom, which are illustrated in Fig. 4.2: these include the axial rotation φ, the linear translation Δz, and the tendon displacement Δl. Let us define the manipulator configuration as a vector $q \in Q \subset \mathbb{R}^3$ containing φ, Δz, and Δl. The forward kinematics of the steerable manipulator is then a function f that takes a design vector d and a configuration vector q and returns the resulting manipulator pose, i.e. $f : (D \times Q) \rightarrow SE(3)$, where $SE(3)$ denotes the Special Euclidean group in 3 dimensions. To describe the kinematics of the steerable manipulator, we use the model from [20]. This model tracks the sheath's bending as a function of the tendon displacement Δl (refer to Fig. 4.2). Briefly, the steerable sheath can be considered as an open kinematic chain composed of a sequence of interleaving cut and uncut segments. Uncut sections are assumed not to undergo any deformation; therefore, their contribution to the kinematics is a simple translation along the local z axis:

$$T_{\text{uncut}} = e^{\hat{\zeta} u}, \text{ with } \zeta = [0\ 0\ 1\ 0\ 0\ 0]^{\mathrm{T}}, \tag{4.5}$$

where u is the notch spacing. The operator ^ in Eq.(4.5) maps twists from $\mathbb{R}^6$ to elements of $\mathfrak{se}(3)$, i.e. the Lie Algebra of the special Euclidean group $SE(3)$. Evaluating the exponential on the right-hand side of the equation yields the corresponding homogeneous transformation matrix $T_{\text{uncut}} \in SE(3)$. For the notched sections, the kinematics model in [20] assumes bending in the shape of a constant curvature arc. The corresponding homogeneous transformation matrix can be expressed in terms of the arc curvature κ and length s (shown in the inset in Fig. 4.2).

$$T_{\text{notch}} = e^{\hat{\xi} s} \text{ with } \xi = [0\ 0\ 1\ 0\ \kappa\ 0]^{\mathrm{T}}. \tag{4.6}$$

The notch arc parameters κ and s are related to the tendon displacement Δl, as it was shown in [20]:

$$\kappa \approx \frac{\Delta l}{h(r_i + \bar{y}) - \Delta l\, \bar{y}},\ s = \frac{h}{1 + \bar{y}\kappa} \tag{4.7}$$

where r_i is the inner radius of the sheath and $\bar{y}$ is the location of the neutral bending plane with respect to the center axis of the sheath. This latter quantity can be calculated using the relations in [20]. Finally, the transformation matrix between the base of the steering section and the distal tip (i.e., frames b and t in Fig. 4.2) is given by:

$$T_{\text{tool}} = \left(\prod_{i=1}^{n} T_{\text{notch}}\ T_{\text{uncut}} \right) T_{\text{distal}} \tag{4.8}$$

where n = 10 is the total number of notches used in our design and $T_{\text{distal}} \in SE(3)$ represents an offset along the local Z axis that accounts for the presence of the end cap and the optical fiber at the tip of the end effector.

To verify that the robot can be controlled using the kinematic model [20], we performed an experiment wherein the actuation tendon was pulled in 0.2 mm increments until all the notches were observed to be fully closed. For tendon pulling, we used a manually-actuated linear slider (Velmex, Bloomfield, NY, USA), which has a resolution of 0.01 mm. After each increment, we took a photograph of the end effector with a digital single-lens reflex camera outfitted with a macro objective (Nikkor 40mmf/2.8 G, Nikon Corporation, Tokyo, Japan) and performed image processing with a custom MATLAB script to measure the bending angle φ. The pixel resolution of each photograph was 4928 × 3624, with a mm-per-pixel ratio of 0.007 mm/pixel.

The experiment was repeated five times. After each trial, we reset the position of the steerable fiber without recording the unbending motion. The average bending angle for a given amount of tendon displacement Δl is displayed in Fig. 4.3. The standard deviation among the 5 trials was < 1°for all values of Δl. As can be seen in Fig. 4.3, there is a linear

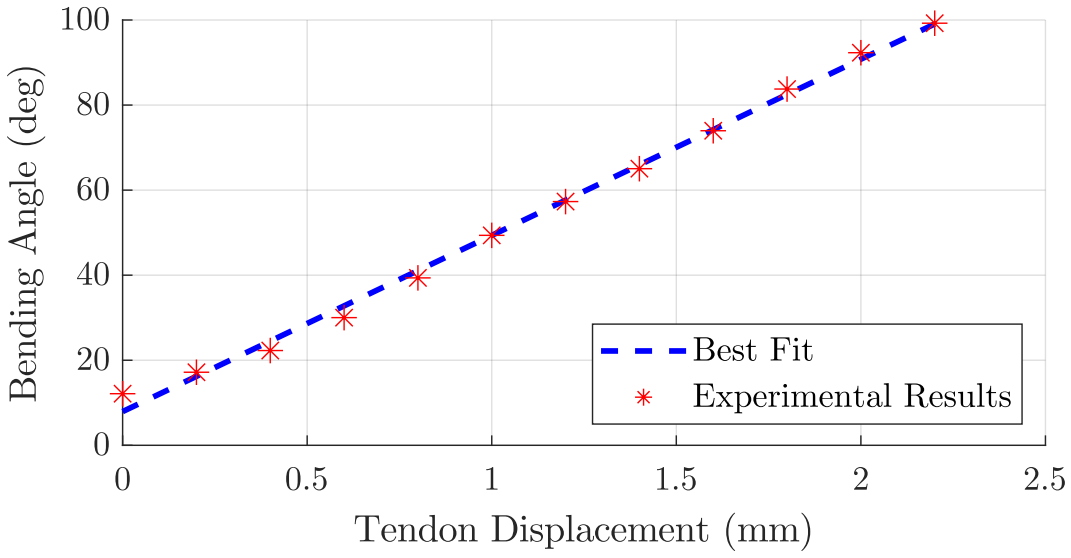

Figure 4.3: *Results of the Kinematics Verification Experiments. The steerable sheath presents an initial pre-curvature of approximately 10°, which we attribute to heating during the laser cutting process.*

relationship between the tendon displacement and the bending angle of the steerable fiber. This result is consistent with the modeling work in [20]. By fitting a linear model, we can map the tendon displacement to the bending angle of the steerable fiber to control its position.

4.1.4 Laser Coupling Module

A 532 nm laser with a power up to 10W was generated from a medical lasers system (Laserscope Aura-i KTP/532, Boston Scientific Co.) and was coupled to an Endostat Surgical Fiber (10-0632, American Medical Systems). With 400 um diameter of glass core and 800um diameter of polymer cladding, this multimode Endostat fiber has limited bending flexibility, with a minimum bending radius of 12 mm. The large core and cladding diameters not only make the fiber difficult to bend and easy to break at small bending radius, but also cause severe power loss (up to 80% of total power) due to the light leakage at the bending position, all of which limit the steerability of the fiber. These challenges were solved by a home-made optical coupling system that couples the laser emitted from the end of the Endostat fiber to a step-index multimode fiber (FP200ERT, Thorlabs) with a 200 um glass core diameter and a 225 um polymer cladding. With only a half of the core diameter of the Endostat fiber, this thinner multimode fiber allows a sharper bending radius of 6 mm and requires less force to bend and thus increases

the flexibility of the probe system. Moreover, the smaller core diameter reduces the influence of bend on the optical transmission, with only 4.5% of optical power loss at 6 mm bending radius. The coupling system consists of two fiber collimators mounted on 6-axis optical stages. a reflective collimator (RC08FC-P01, Thorlabs) collimates the laser emitted from the end of the Endostat fiber, and the collimated beam was then focused and coupled to the step-index multimode fiber by an achromatic straight collimator (F950FC-A, Thorlabs). By easily adjusting the optical stages, we have achieved 54.5% of the laser coupling efficiency between the ends of the Endostat fiber and thinner fiber. The performance of the system is consistent with minimum effort of maintenance such as realignments over months of usage. The detailed characterization of the coupling system can be found in [71]. The developed coupling system enables the light to be delivered by a thin multimode fiber, providing flexibility to the probe tip for precise position and steering control with minimum optical power loss.

4.2 Simulations

Following the methodology outlined in section 3.3, we estimate the reachable workspace achieve by the steerable manipulator. First, we generate 10,000 random endoscope+fiber configurations using the Rapidly-Exploring Random Trees (RRT) algorithm. From each of these reachable configurations, we run a ray-casting algorithm to simulate the application of laser pulses. We generate 1,000 virtual rays from the tip of the fiber in a cone that mimics the laser beam. With each of these rays, we use the Moller- Trumbore ray-triangle Intersection algorithm to detect what faces of the STL larynx model are visible in a direct line of sight. Results are shown in Fig. 4.4.

To evaluate the benefits of adding steering to laser fibers, we compare our results with reachable tissue maps previously calculated in section 3.4 for clinical non-steerable laser fibers (”Traditional Fiber” in Fig. 4.4). Our new steerable fiber was found to provide significantly more extensive access to the larynx anatomy, compared to traditional clinical fibers. Enhanced coverage is observed particularly in the area surrounding the vocal folds, which as was noted earlier, can be challenging to reach with current clinical fibers. Table 4.2 shows numerical results, indicating that being able to bend laser fibers more than doubles the amount of accessible tissue.

Table 4.2: *Tissue Coverage Estimated in Simulation*

	Traditional Fiber [cm^2]	**Steerable Fiber [cm^2]**
Larynx 1	8.99	20.65
Larynx 2	8.51	19.30

4.3 Phantom Experiments

To verify the steerable fiber ability to access hard-to-reach locations inside the larynx, we performed a set of experiments using a 3D-printed phantom model of the human larynx. The phantom model, pictured in Fig. 4.5, was printed with a Form 2 printer (Formlabs, Somerville, MA, USA). This is the same anatomical model showed earlier in Fig. 4.4 and labeled "Larynx 1." The model was printed as a two-piece phantom, so that we could open it and take pictures to document the deployment of the steerable fiber (see Fig. 4.6). To enable registration between the 3D-printed phantom and its STL model, we created four fiducial points, as shown in Fig. 4.5.

The experiments were carried out as follows: first, the endoscope was deployed into the phantom model so that the steerable fiber probe would navigate in plane with the phantom surface. With the endoscope stationary, we deployed the steerable fiber into the phantom model and visually aligned it with the surface of the model. The steerable fiber was controlled using a bench-top control panel with buttons [74] for each of the DoF described earlier in section 4.1.3. The steerable fiber was maneuvered to follow the profile of the tissue surface, scanning from above the vocal folds to the region immediately below, as shown in Fig. 4.6.

Throughout each experiment, we tracked the location and orientation of the end effector's tip from images (using the same camera and lens previously used in the kinematics verification experiments), and then used the registration between the phantom and its STL model to project a virtual model of the robot in the STL space. This enabled us to use the same ray casting technique described earlier in section 3.3 to identify the tissue accessed by the fiber. Results are shown in Fig. 4.7, and they show our manipulator's ability to reach the regions immediately above and below the vocal folds, which are currently out of reach with traditional clinical fibers.

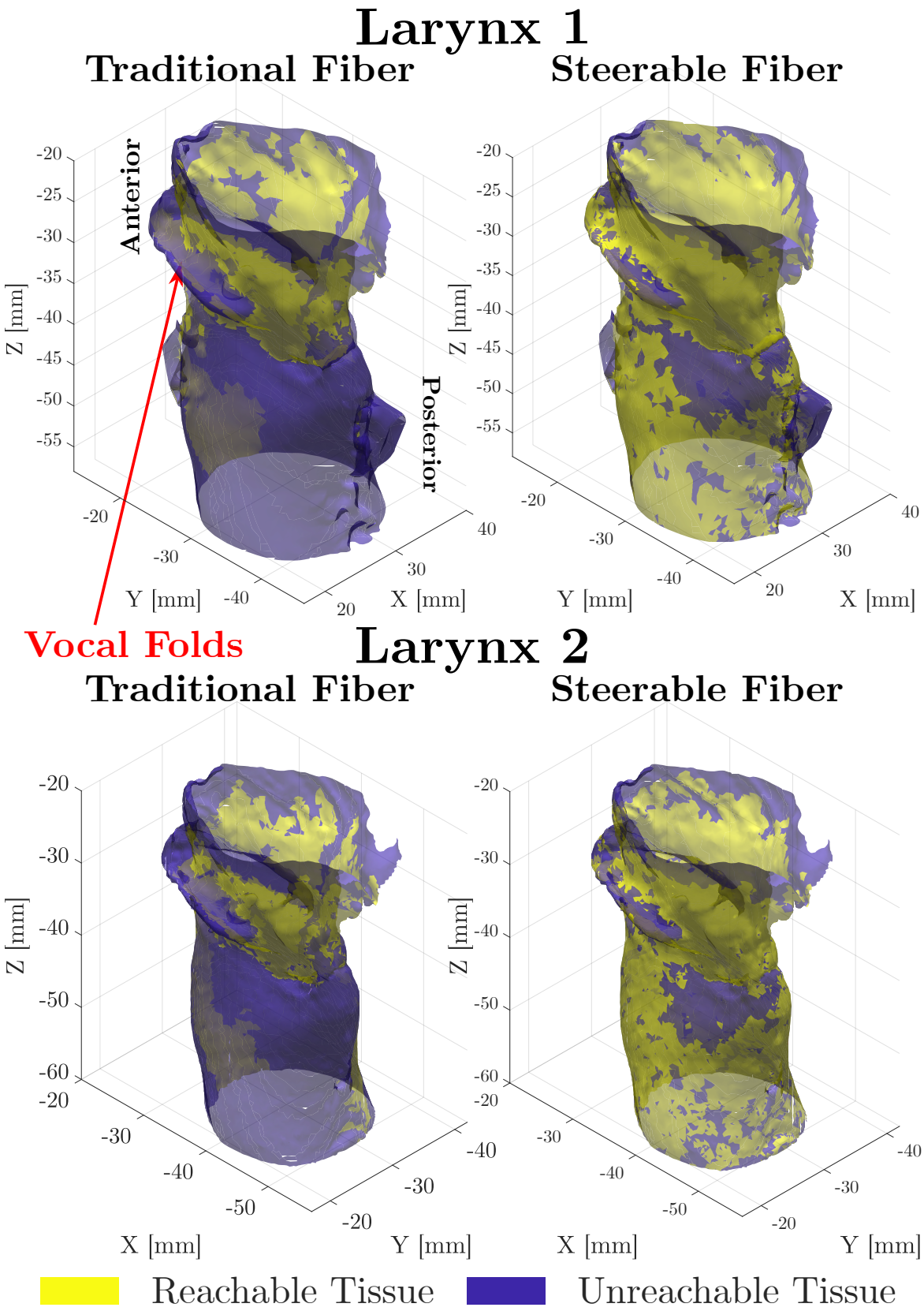

Figure 4.4: *Reachable tissue in two different larynx models. Here, "traditional fiber" refers to the non-steerable fibers currently in clinical use. "Steerable fiber" indicates our new proposed device.*

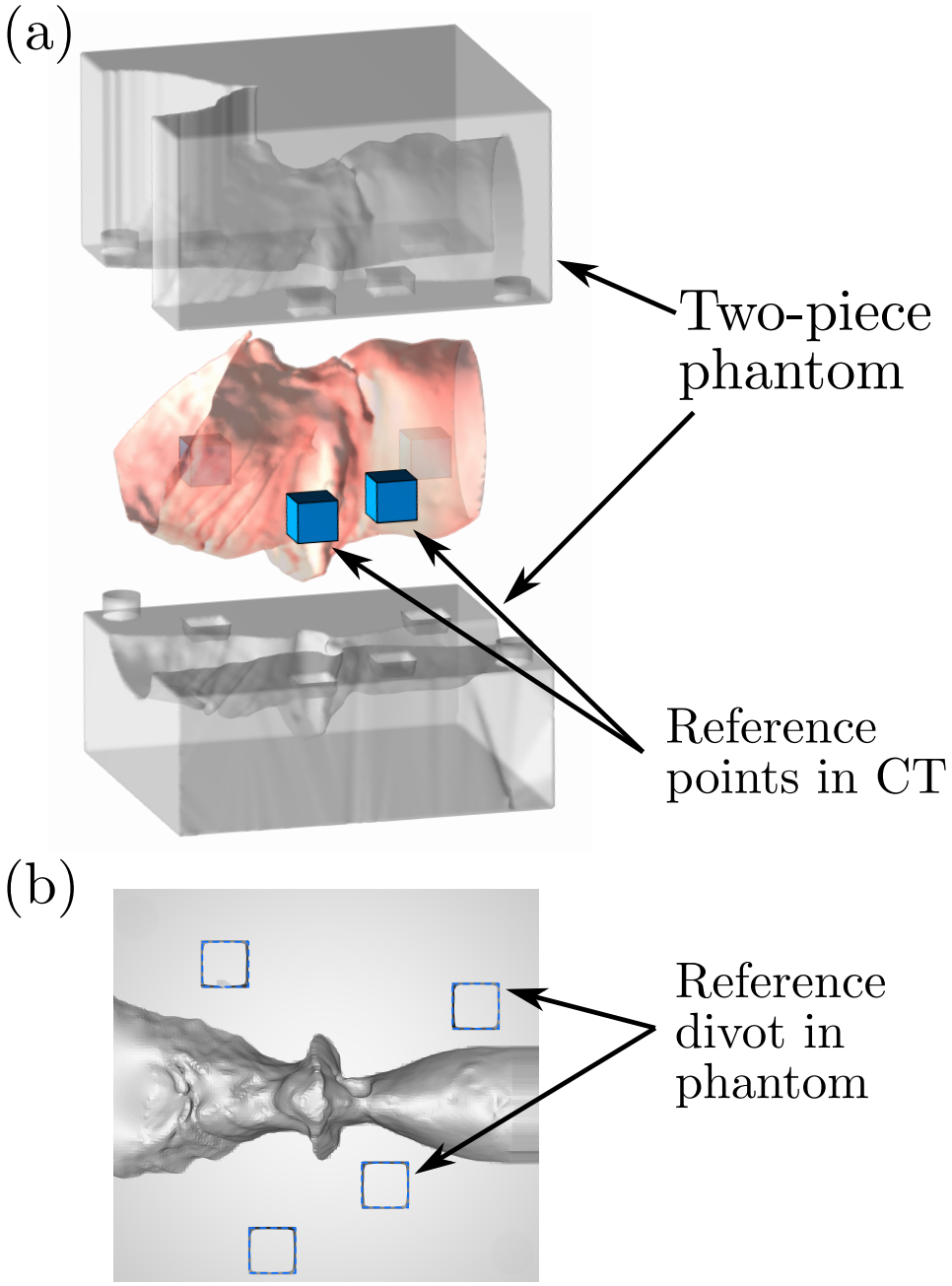

Figure 4.5: *3D printed phantom used in the experiment. (a) An exploded view of the two-piece phantom and larynx mesh model used to generate the phantom. The reference points are shown as blue cubes and were used for registration with the phantom. (b) A planar view of the phantom. The divots (outlined in blue dashes) corresponding to the reference points in the CT scan were localized in the photographs during the experiment.*

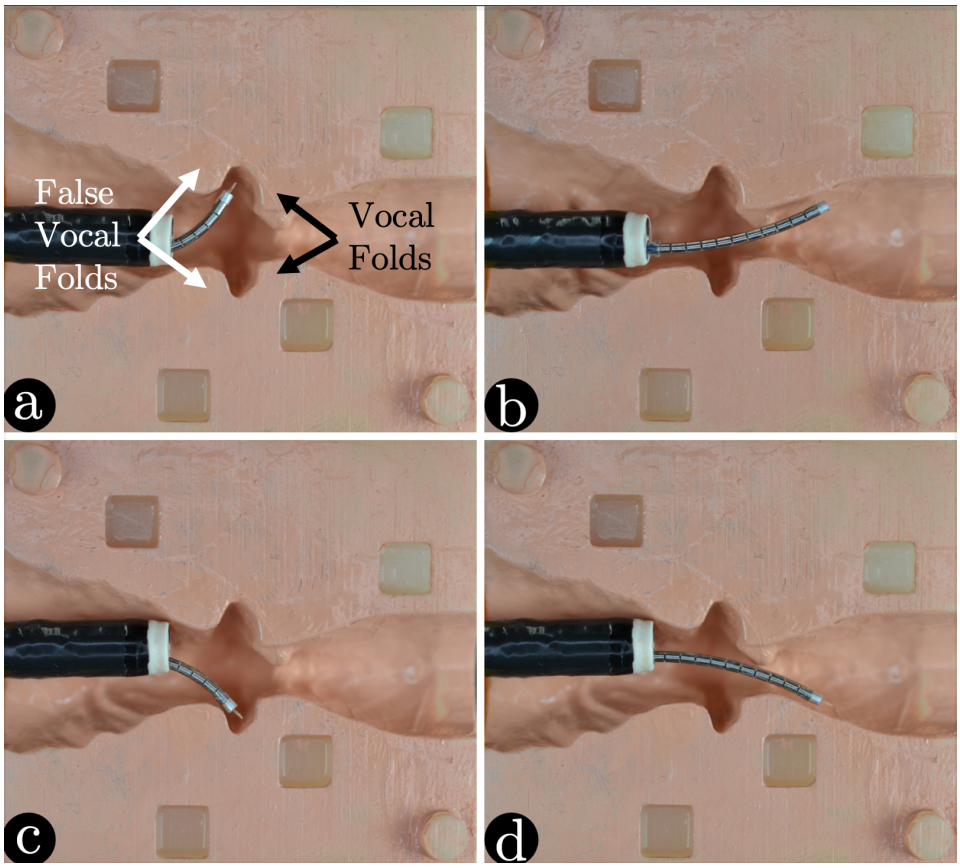

Figure 4.6: *Examples from the phantom experiments can be seen in (a)-(d). The goal was to target positions in between the false and true vocal folds, as well as beneath the right and left vocal folds. Panel (a) and (b) demonstrate the limits for the right vocal fold, and panels (c) and (d) indicate the limits for the left vocal fold.*

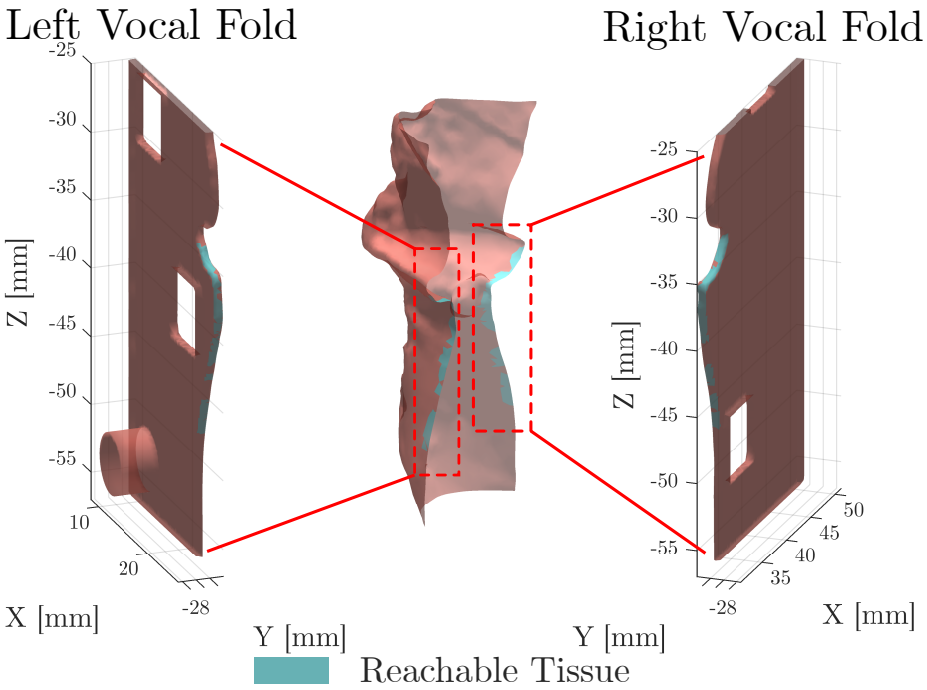

Figure 4.7: *The results of the phantom experiment are shown here for the left and right vocal folds. The steerable probe allows the optical fiber to reach areas inside and beneath the vocal folds.*

CHAPTER 5

USER INTERFACE

In this chapter, we describe the development of a handle prototype manipulator to control the Steerable Optical Fiber for in-office laser surgery. The objective is to provide physicians with a control manipulator to 1) operate the 3 DoF of the SOF (translation, rotation, and bending) and 2) minimize the impact on the surgical configuration for in-office laser surgery.

In the subsequent sections, we present the manipulator's design considerations, mechanical configuration, and control architecture, describing its operational capabilities and clinical application. Additionally, we report on preliminary validation to assess the functionality and feasibility of the manipulator in a simulated clinical scenario to treat laryngeal tumors.

5.1 Single-Handle Controller

The design of the single-handle controller prioritizes the integration into the current surgical configuration while providing intuitive and efficient control over the steerable optical fiber's three degrees of freedom as shown in Fig. 5.1.

5.1.1 Design Considerations

The control manipulator is designed to enable a single-hand operation to control: 1) the insertion and retraction of the SOF into and out of the working channel of the endoscope

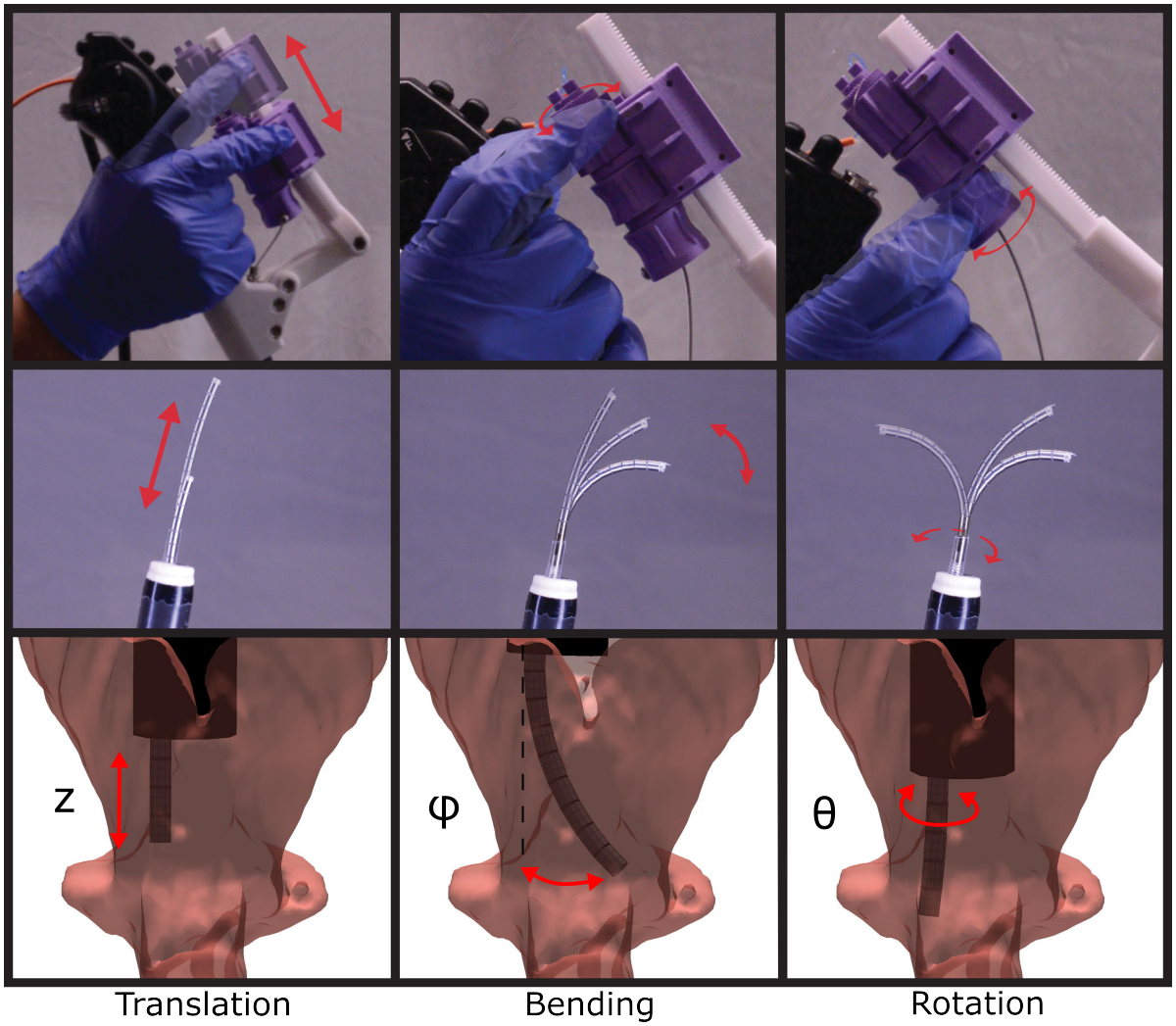

Figure 5.1: *Illustrates the single-handle device operation (from top: view of the control unit, detailed view of the actuated DoF, and the resulting probe motion within a larynx rendering): (left) Operation of the cartridge along the axial shaft resulting in the z displacement of the probe, (middle) rotation of the bending knob actuates the probe in the φ direction, (right) the distal st of rotation knobs actuate the probe in ϑ.*

Δz, 2) the axial rotation of the instrument inside the larynx ϑ, and 3) the tip bending φ. We outlined the design considerations in the following summary:

Operation Ranges: To maximize the reachability of the SOF at the distal end of the endoscope, the controller must allow for the following mechanical ranges.

1. **Rotation:** Able to be continuously rotate in both directions.
2. **Linear:** Able to extend 0 – 40 [mm] out the distal end of the endoscope's working channel.

3. **Bending:** Able to completely bend the SOF.

Control Manipulation: The device should enable the user to manipulate all three DOFs of the SOF (bending, translation, rotation) using the same hand already holding the endoscope. This allows the clinician to maintain the use of their other hand to hold the flexible tube at the insertion point and preserve the traditional operational workflow.

5.1.2 Mechanical Configuration

The prototype is shown in Fig. 5.2. The device is a 3D-printed mechanism that houses the components for steerable fiber manipulation. We have integrated a cartridge mechanism that traverses along a linear shaft, facilitating the translation of the steerable fiber within the endoscope. The cartridge adjusts the insertion depth, ensuring optimal positioning for laser delivery at the surgical site.

For bending and rotation, our design incorporates a set of control knobs, positioned for intuitive operation by clinicians. The bending knob allows clinicians to deflect the fiber by up to 90 degrees, thereby enhancing maneuverability and access to hard-to-reach areas within the larynx. Simultaneously, the rotation knob provides clinicians with total control over the fiber orientation, facilitating, 360-degree rotation in both clockwise and counterclockwise directions.

To complete the assembly of our control system we require a shaft to connect the proximal control unit to the distal steerable fiber. The shaft must be flexible to navigate through the scope yet torsional rigidity to ensure an effective rotational transmission from the controller to the distal steerable fiber. However, balancing both bending compliance and torsional stiffness in a single shaft presents a significant engineering challenge. To address this challenge, we conducted a comparative study of three shaft options: two off-the-shelf spring coils shown in Fig. 5.3 (a) and (b) and a custom-manufactured torsional spring depicted in Fig. 5.3 (c).

5.1.2.1 Spring Shaft

To determine the appropriate shaft option for our controller, we investigated two off-the-shelf spring coils and one custom-made torsional spring commonly employed in medical devices. The shaft must be sufficiently small to navigate the endoscope's narrow working channel (2 mm), while also offering sufficient inner diameter to accommodate both the tendon actuator (0.1 mm) and the optical fiber (0.5 mm). The first spring coil examined, depicted in Fig.5.3 (a), is the Spring Guide (Templeman Co, Plainville, CT,

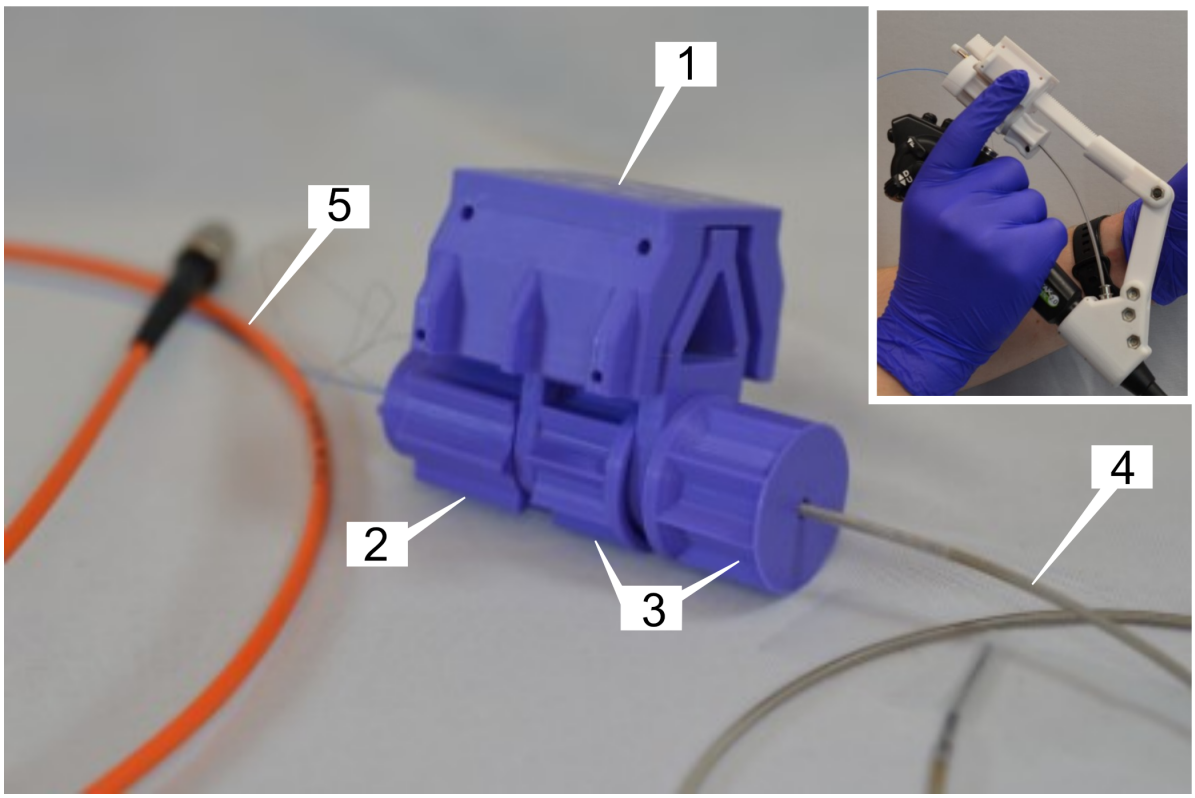

Figure 5.2: *Illustrates the elements to assemble a single-handle controller. (1) Cartridge unit. It connects to a triangular rial (depicted in the top right inset) facilitating the translation of the SOF within the endoscope. (2) Bendig Knob. The tendon-wire is attached to the bending knob. The rotation of the knob causes a linear displacement to pull the tendon wire enabling the SOF to bend. (3) Rotational knobs. They allow unrestricted rotation in both directions. A torsional spring shaft is rigidly attached inside the right knob with a* 2 mm *set screw, therefore, any rotation in the knob will result in an equal rotation at the SOF. (4) Torsional spring shaft. It connects the single-handle controller to the distal SOF. The torsional spring shaft needs to be flexible to navigate through the endoscope working channel as well as to provide torsional stiffness to transmit the rotation from the control knob to the distal SOF. (5) Optical fiber described in section 4.1.1.2. The inset show the manipulation of the single-handle controller.*

USA), constructed from stainless steel with an outer diameter of 1.32 mm and an inner diameter of 0.66 mm. Our second option is the Pentax Forcep (Pentax, Tsutsujigaoka, Japan), shown in Fig.5.3 (b), a product of the same company responsible for the endoscope utilized in our study. Lastly, we assessed a custom-made torsional spring coil (Sawane Spring, Hamamatsu, Japan), shown in Fig.5.3 (c). The torsional spring is crafted from stainless steel, featuring 8 filars and 3 layers designed to enhance torsional rigidity, with outer and inner diameters measuring 1.60 mm and 0.8 mm respectively.

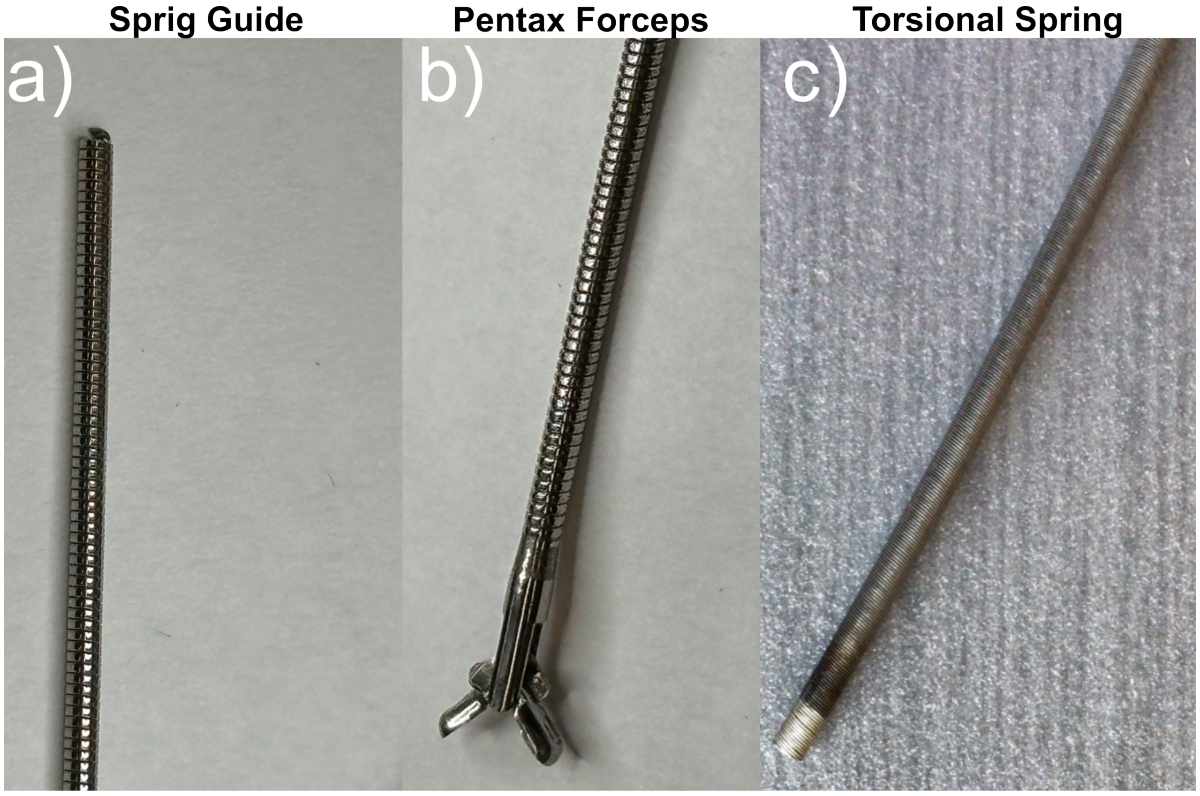

Figure 5.3: *Spring coils shaft to connect the control unit to the distal SOF. (a) and (b) are off-the-shelf spring shafts for medical applications while (c) is a custom-made torsional spring designed to enhance torsional rigidity.*

To test each spring shaft, we positioned the endoscope into a custom bench to hold it in place. The endoscope working channel is placed into the slots of the two black supports in a rounded 90-degree bend to mimic the anatomical bend from the endoscope's insertion point to the vocal folds. Three clear, acrylic end caps can be switched out to test different endoscope tip angles. We tested with 0, 60, and 90-degree bends. Fig 5.4 illustrates the experimental setup previously described.

Each spring coil is inserted through the black rotary stage into the endoscope working channel through a white custom rotary stage to measure the rotation at the distal end. Then we rotated the proximal end by increments of 10 degrees until complete 360 degrees. At each increment, we measured the rotation at the distal end. For each spring coil, the experiment was repeated twice (clockwise and counterclockwise).

Fig. 5.5 illustrates the transmission level at the free end. The data indicates the custom torsional spring provides nearly one-to-one transmission, suggesting notable efficiency in transmitting motion from the controller to the distal end. Moreover, the

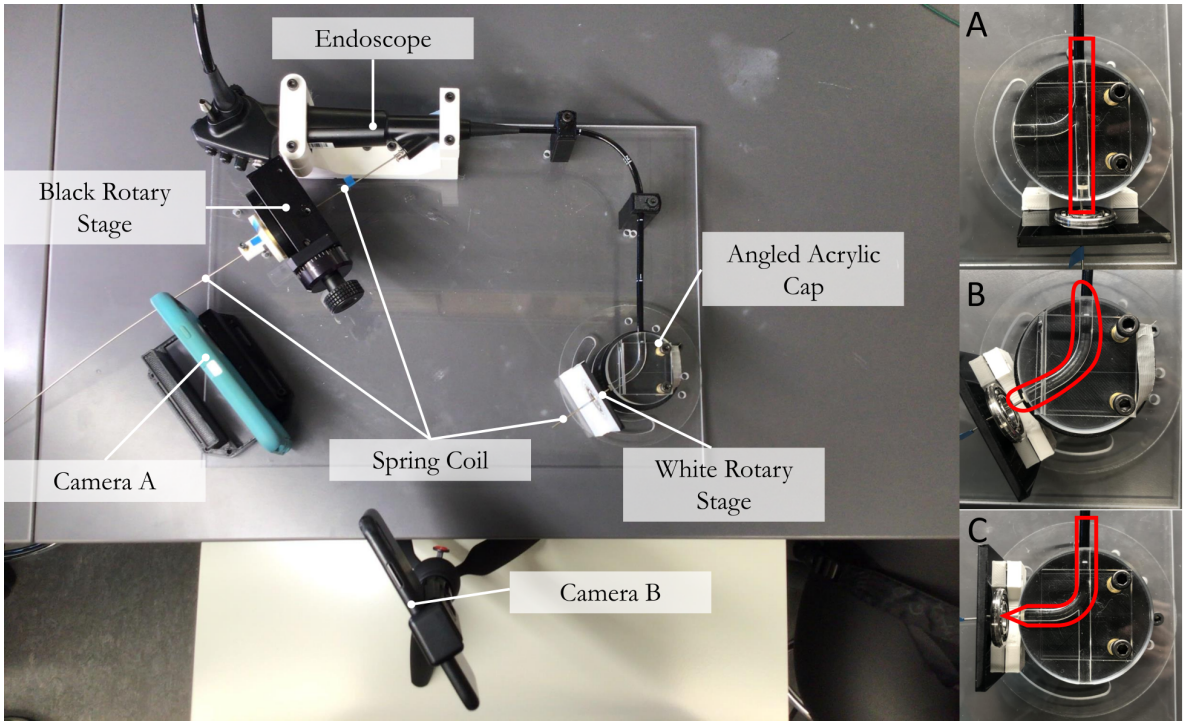

Figure 5.4: *Experiement Setup to evaluate the rotational transmission of the spring coil shafts. The endoscope is fixed into the custom white jig. The endoscope's working channel is placed into the slots of the two black supports in a rounded 90-degree position to simulate the anatomical bend from the endoscope's insertion point to the vocal folds. The tip of the endoscope is held in place with acrylic end caps that can be switched to test different endoscope tip angles: A) 0 degrees, B) 60 degrees, and C) 90 degrees. The spring coil is inserted through the Rotary stage and passes into the endoscope working channel all the way through the white custom rotary stage to measure the rotation.*

spring shaft demonstrates robustness across various bending configurations of the scope. These findings underscore the potential of the custom torsional spring as an optimal choice for our application.

While our analysis indicates promising results in terms of torsion stiffness, we consider it important to address the flaws observed in rotation behavior. We aim to elucidate the process by which we achieve a complete 360-degree rotation and highlight the underlying factors contributing to deviations from ideal linear behavior. The results shown in Fig. 5.6 suggest the presence of friction and potential torsional windup, wherein energy is stored and later released. This phenomenon introduces variability and non-linearity into the rotational movement, impacting the precision and consistency of control. While this may not pose a significant challenge when the device is manually controlled by a physician, as they can intuitively adjust based on visual feedback, it could become a

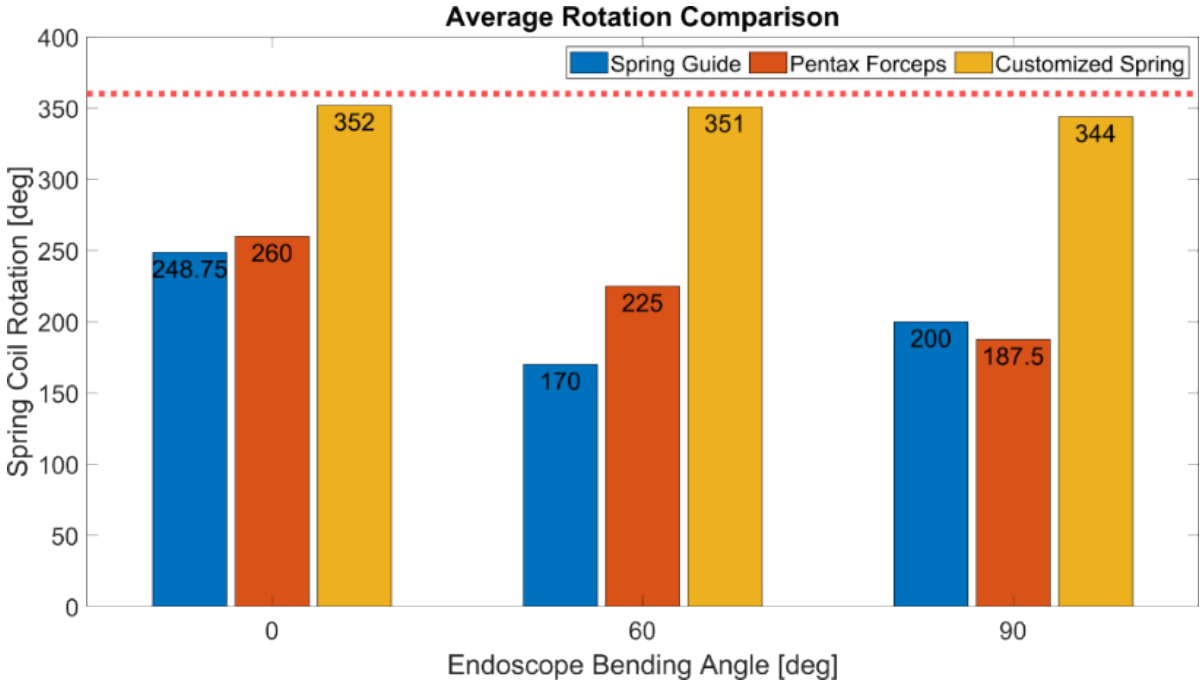

Figure 5.5: *Results of the rotational study of the spring coils. The plot shows the average rotation of each spring coil at different configurations of the endoscope tip.*

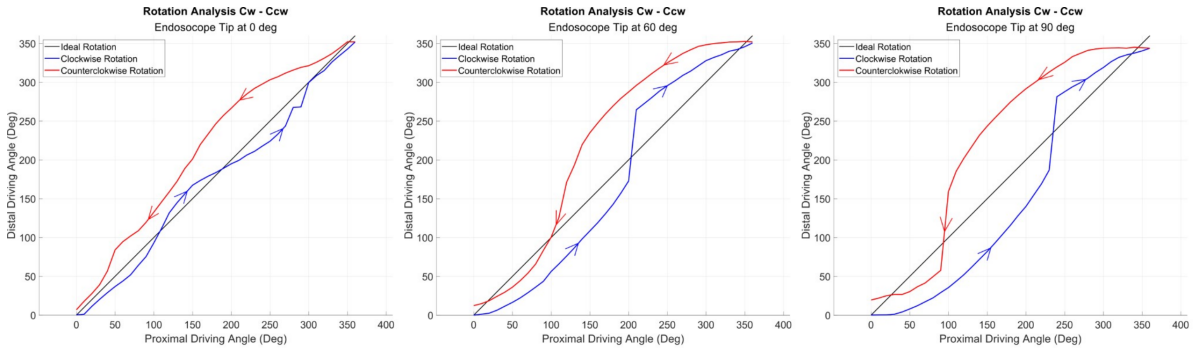

Figure 5.6: *Validation experiments depicting the performance of the spring under various endoscope configurations. The spring coils undergo clockwise rotation until completing a full 360-degree rotation (as indicated by the blue line). Conversely, the red line shows counterclockwise rotation from the last position of the spring coil last until returning to 0 degrees.*

critical issue if the probe transitions to robotic control in the future. In such a scenario, precise control mechanisms would be essential to manage and mitigate the effects of torsional windup, ensuring consistent and accurate rotational movement.

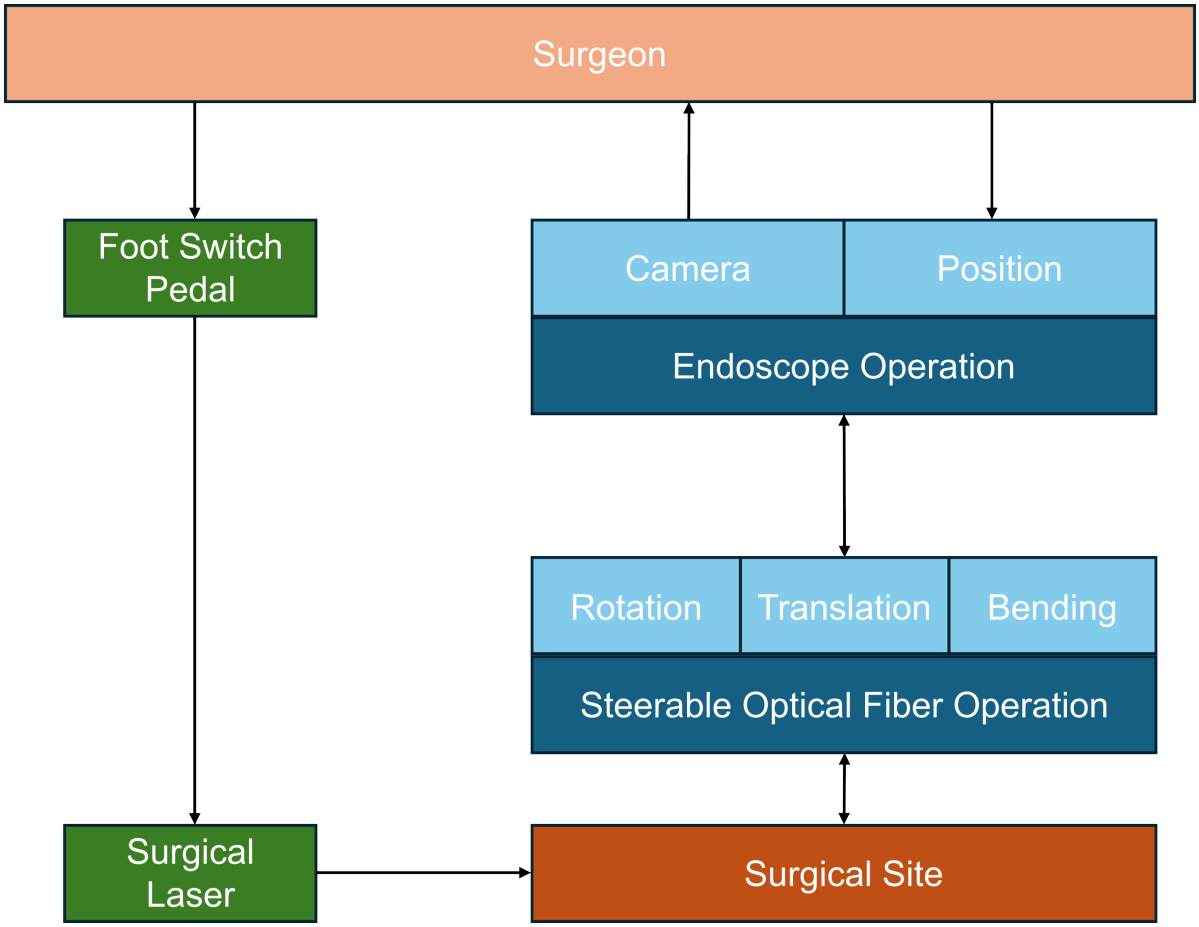

Figure 5.7: *Control Architecture to operate the single-handle controller.*

5.1.3 Control Architecture

The control process of the steerable optical fiber involves the active participation of the surgeon. Fig. 5.7 provides a schematic depiction of the control process. Surgeons maneuver the endoscope into the desired location within the larynx, ensuring optimal positioning for the upcoming procedure. Once in position, the surgeon utilizes the single-handle controller to operate the steerable optical fiber, directing its movements to perform the surgical ablation over the diseased tissue.

5.2 Materials and Methods

To assess the efficacy of the steerable optical fiber, we replicate the surgical environment within an office setting for a controlled experiment. The experimental configuration, as depicted in Fig. 5.8 employs a commercial Laserscope KTP Aura-i system (Boston

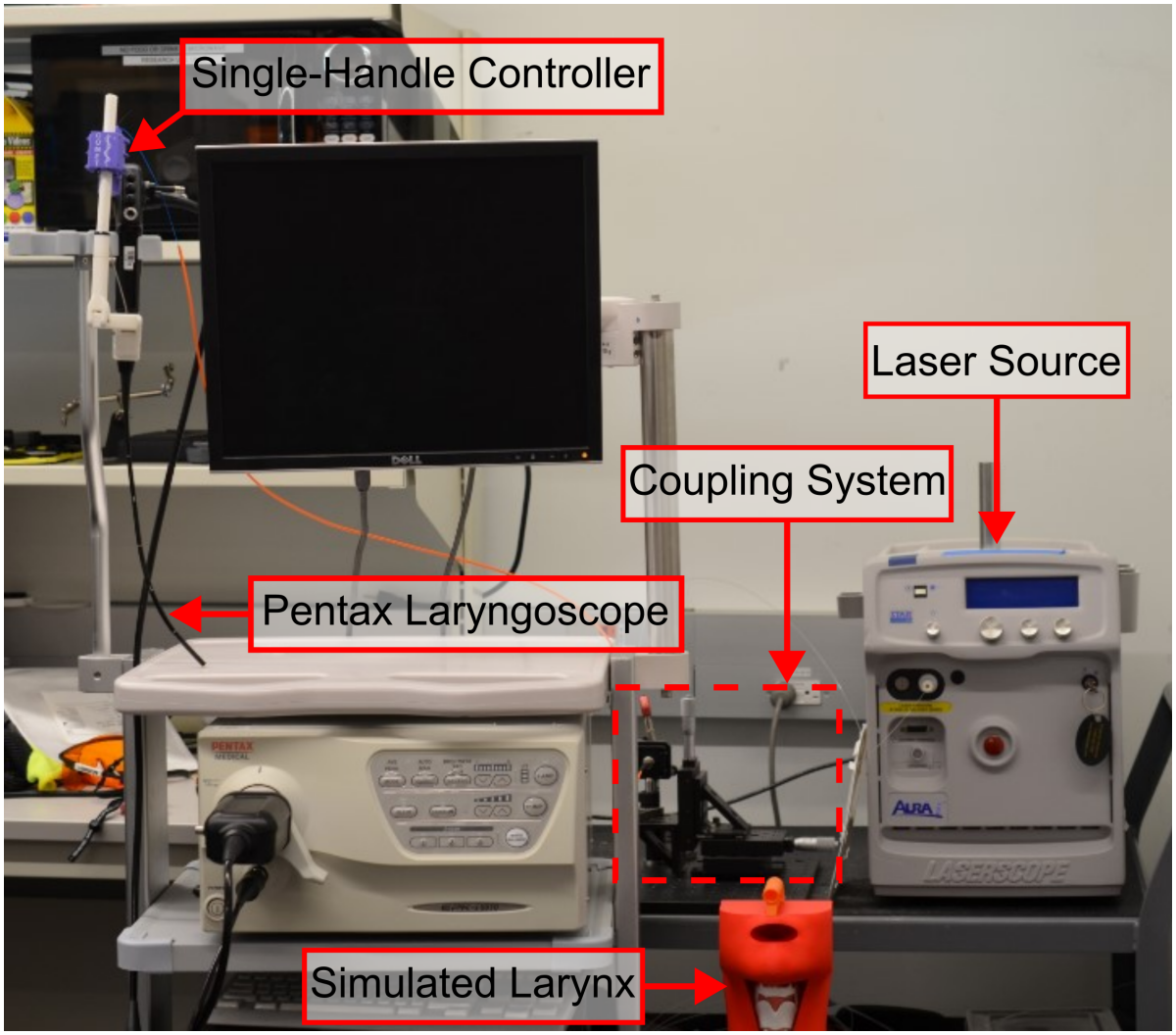

Figure 5.8: *Experimental Setup. The Endoscope is inserted into the simulated Larynx manikin. The user will operate the single-handle controller inside the larynx. When the user identifies a target within the larynx will press a footswitch (not displayed in the figure) to activate the KTP laser source. Then the light is coupled into the multimode fiber to deliver energy to the surgical site.*

Scientific Co.) operating at a wavelength of 532 nm. The optical fiber coupling system, developed by Zhu and colleagues [71], facilitates the coupling of light from an Endostat fiber into a smaller multimode fiber, enabling precise steering of the endoscopic probe in confined spaces. The coupling system achieved a power coupling efficiency of nearly 50%. We integrate the commercial Pentax laryngoscope alongside the single-handle controller, allowing users to manipulate the instruments to access various targets within the larynx. Furthermore, to replicate realistic conditions, we utilize a 3D-printed laryngeal simulator that we modified from [54].

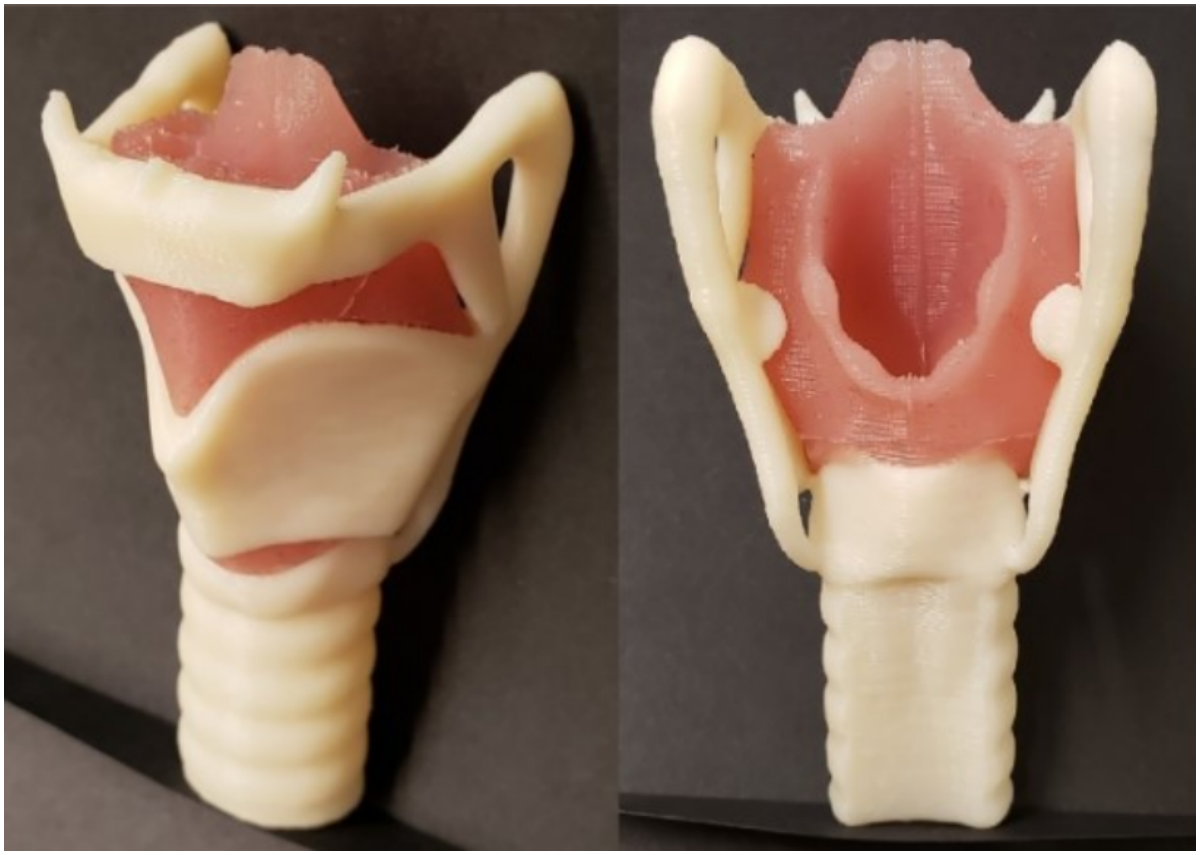

Figure 5.9: *Laryngeal simulator. It encompasses a human-size silicone Larynx and a 3D-printed cartilage. Reproduced from [54]*

We utilized a three-dimensional model of the larynx, originally developed by Mark Lee and colleagues [54]. They established a protocol for manufacturing silicone larynx models as depicted in Fig. 5.9.

In our study, we adapted this model to create our silicone larynx replicas, drawing from the same dataset referenced in our simulations in section 3.1. Additionally, we cut a series of dives, shown at the left of Fig. 5.10, which allows us to place small thermal paper marks that would turn black upon being hit by the laser, providing a visible indication of ablation. Furthermore, we developed a modified model featuring protuberances representing diseased tissue (Fig. 5.10). Upon exposure to the laser, these protuberances undergo a color change, allowing for the visualization and assessment of the laser ablation on the simulated tissue.

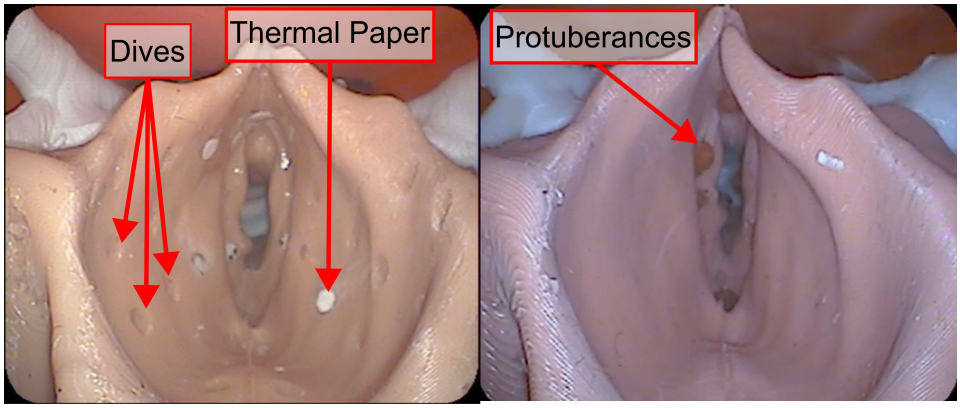

Figure 5.10: *Top view of the silicone Larynx. (Left) It shows a series of dives crafted in the larynx to fix thermal paper. The thermal paper helps to identify if the surgical site is fired. (Right) Updated version of the silicone larynx that simulates diseased tissue as protuberances. The protuberances change color when they are fired by the laser.*

5.3 Preliminary Validation

The preliminary evaluation aims to assess the feasibility of utilizing our Steerable Optical Fiber to target hard-to-reach locations within the larynx. We conducted a comparative analysis of the operational efficacy between the traditional fiber and our Steerable Optical Fiber.

Participants, without medical training, were tasked with firing several predefined locations within the larynx. Fig. 5.11 illustrates the sequential process of firing the red-marked target. The user, maneuvering the endoscope and fiber as necessary, attempts to fire the target. However, the target has no visible marks, leading the user to fire the laser twice. While adjusting the position of the endoscope and fiber, the user identifies a more accessible blue-marked target. Subsequently, the user withdraws the fiber to enhance visualization of the desired target and readjusts their position. During this process, the user discovers that the green-marked target is more readily accessible. After several attempts, the user successfully fires at the initial red target after 74 seconds.

In contrast, when utilizing our steerable optical fiber (Fig. 5.12), the user employs a different approach. They maneuver the endoscope and the SOF to position themselves as close as necessary to the target circled in red. Despite the fiber being bent at an angle of around 10 degrees, the user discovers that the golden-marked target is more readily accessible. From this favorable position, the user realizes that they only need to manipulate the fiber upwards to effectively fire the original red-marked target. The total time to complete the surgical task using our steerable optical fiber is 12 seconds. This

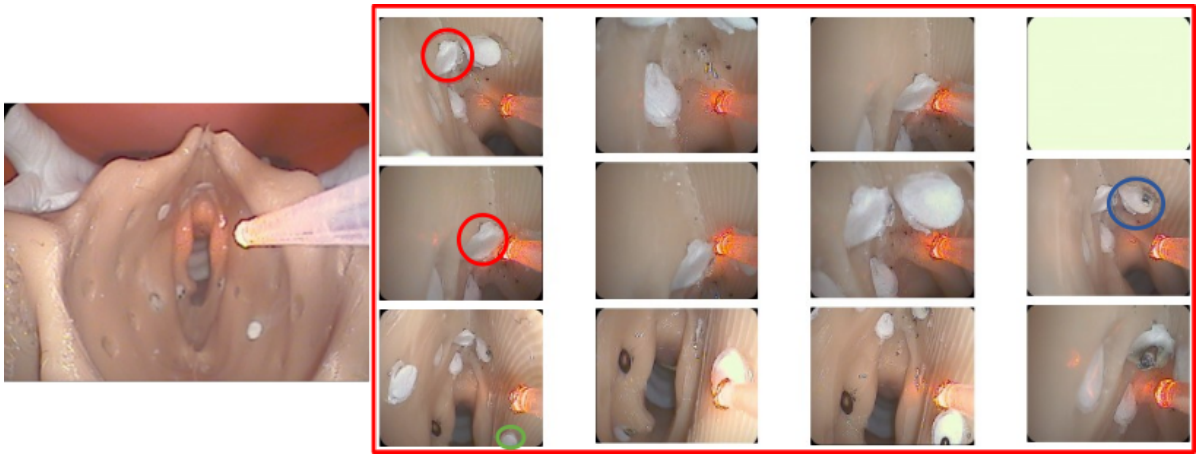

Figure 5.11: *Sequence to fire a hard-to-reach target (circle in red). Read the sequence starting at the top left to the right. First row: the user found the desired target and moved the endoscope and the fiber to get as close as needed to fire the target as is shown in the last image. Second row: The desired target is not marked and the user shoots the laser 2 more times and barely hits the desired target's edge. The user found himself in a better position to fire the target (circle in blue) near the desired target and mark it. Third row: The user extracts the fiber to better visualize the desired target and relocate his position. However, the user found the target marked in green to be more accessible. Thus, the user fires this target. Finally, after several attempts to aim the target marked in red for 20 seconds more, the user finds a suitable position to fire the desired target. The time recorded since the user finds the desired target (marked in red) to fire it is 74 seconds.*

scenario highlights a distinct advantage of utilizing our fiber: when near a target, the conventional approach necessitates positioning the camera extremely close to the tissue to attempt to fire the laser. This limited field of view requires constant repositioning of the instrument. In contrast, deploying our steerable fiber allows the user to maintain certain distance, affording a broader view of the surgical site and facilitating better perception and surgical awareness.

5.4 Reachability Validation

The overarching goal of the reachability study is to assess the efficacy of the steerable optical fiber in accessing predetermined targets within the larynx. In this study, we employ three-dimensional larynx models featuring six protuberances designed to simulate tumors, as detailed in section 5.2.

The reachability study employs the same criteria as those utilized in our simulations analysis described in section 3.3, comprising two primary considerations: first, we assess

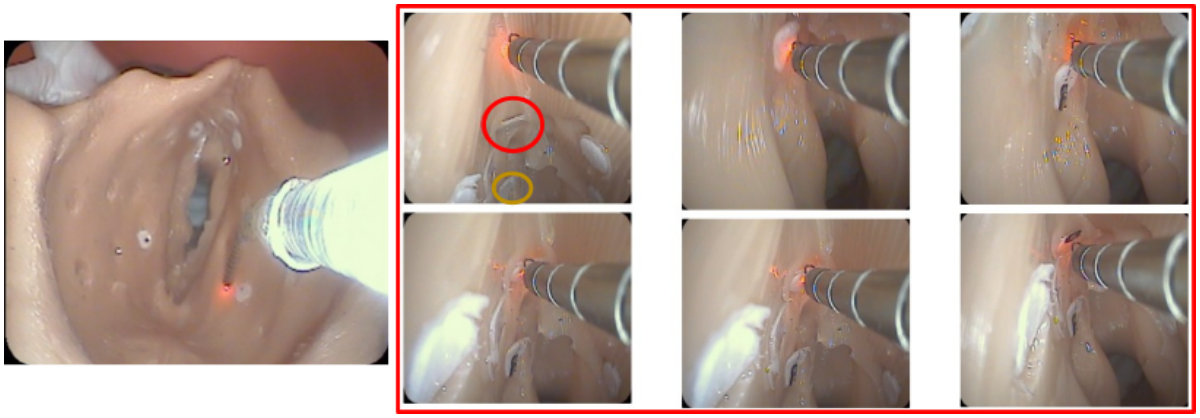

Figure 5.12: *Sequence to fire a hard-to-reach target (circle in red). Read the sequence starting at the top left to the right. First row: the user found the desired target and moved the endoscope and the SOF to get as close as needed to fire the target. The user set the default bending of the SOF which is around 10 degrees to aim the target. However, the user finds it easier to aim the target marked in blue, close to the desired target. He relocates the SOF and fires the target marked in blue as the last image shown. Second row: The user moved SOF up to aim the original target and he found himself in a more comfortable position to fire the target this time. Finally, the user successfully hit the target. The time recorded since the user find the desired target (marked in red) to fire it is 12 seconds.*

whether we can effectively direct the optical fiber towards the lesion and subsequently fire it. Then, we evaluate whether we can adequately visualize the actions of the optical fiber during firing. If both conditions are met, we classify the target as valid.

For instance, when targeting a tumor situated below the right vocal fold as Fig. 5.13 illustrates, we assess the scenarios involving both the traditional straight fiber and the steerable fiber. While we may successfully reach some lesions with either fiber type, there are certain locations, such as the one positioned lower the vocal fold, where the straight fiber proves inadequate. In such cases, despite being able to reach the lesion, our inability to visualize the fiber's actions during firing makes the location non-reachable when using the straight fiber. However, with the steerable fiber, we overcome this limitation, allowing us to effectively navigate and target otherwise inaccessible areas.

Each target shown in Fig. 5.14 is assigned a numerical value ranging from 0 to 1, with 0 indicating that it does not meet the specified criteria and 1 signifying that it does. The cumulative value of these assessments is then calculated, with a maximum value of 3 indicating that the target is both reachable and visible, thereby allowing for laser firing. The performance outcomes of the traditional fiber and the steerable optical fiber are presented in Tables 5.1 and 5.2, respectively.

The analysis reveals that the steerable optical fiber offers advantages in only one

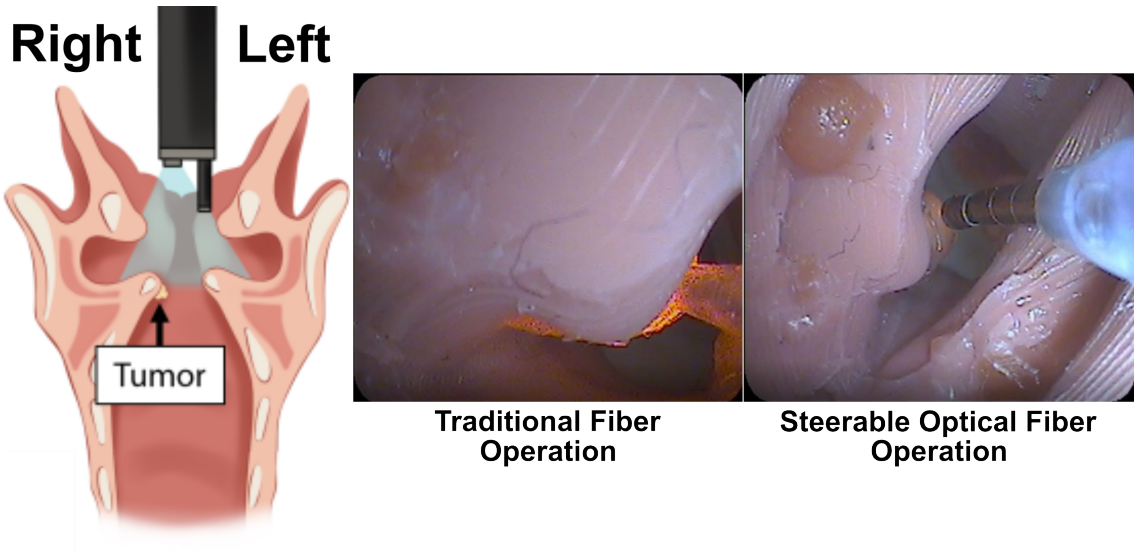

Figure 5.13: *Reachability Validation. The illustration at the right shows the position of the tumor ("protuberance") that we aim for. The subsequent pictures show the footage of the endoscope camera at the moment to fire the tumor with the Traditional Fiber and with the steerable Optical Fiber.*

specific location, below the vocal folds, whereas the remaining targets are accessible with either fiber type. Additionally. it appears the user has a better visualization of the workspace using the SOF which facilitates the aiming of the targets. Using the SOF, the user found a suitable position to fire some targets in a shorter time compared with the traditional fiber. It is important to acknowledge certain limitations in our study, particularly regarding the larynx model utilized.

While the model provides a suitable representation of the larynx, it remains static and fails to account for the natural movement exhibited by awake patients, simplifying the operation of both the traditional fiber and the steerable optical fiber. Additionally, the model fails to account for the folding tissue structure present in the human larynx, particularly in the region of the epiglottis and supraglottis, which further complicates access to certain surgical sites in the area of the vocal folds. Incorporating these considerations into future models would provide a more accurate assessment of the reachability of the steerable optical fiber, enhancing our understanding of its potential benefits in clinical practice.

Regarding the usability of the single-handle controller, first, as is expected given the current control system, the operation of the SOF requires an adaptation process. The users switch from controlling a 3 degrees of freedom (DoF) instrument to operating a 6 DoF. Second, the users sometimes found the bending control unresponsive. Thus setting

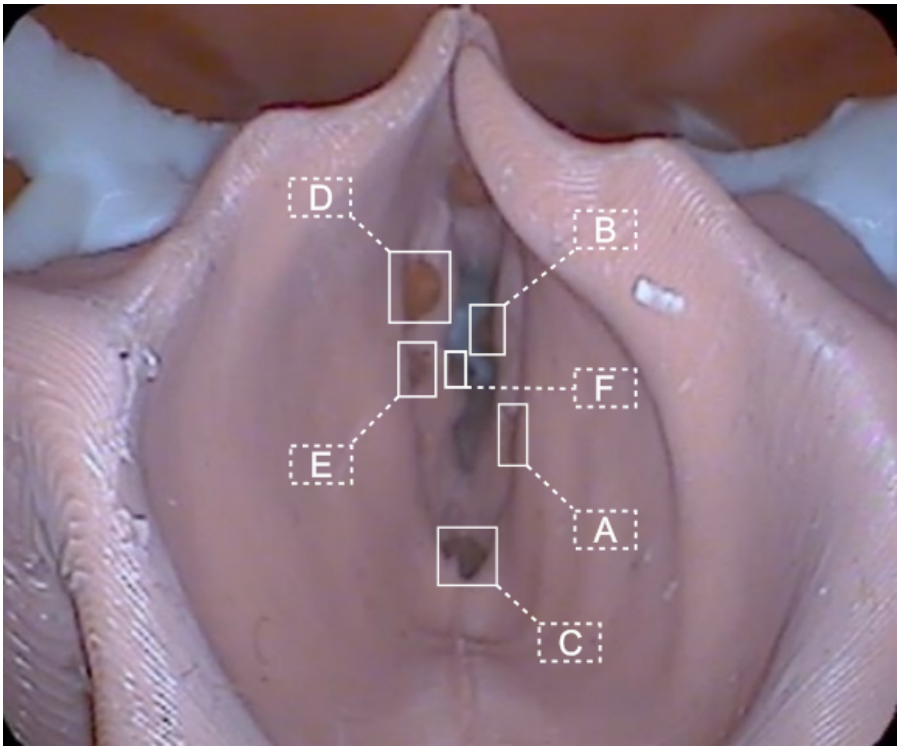

Figure 5.14: *Top View of the silicone larynx identifying six targets to aim for with the Traditional Fiber and with the Steerable Optical Fiber.*

the SOF to its default bending was enough to complete the task. A potential option could be to redesign the SOF to bend in a different pattern. Finally, the user underutilized the translation DoF to navigate and reach the targets. This is attributed to a lack of experience and, in a certain way, the user tends to use the system as it did with the traditional fiber.

Table 5.1: *Reachability Analysis of the Traditional Fiber*

Target Number	Target Description	Difficulty Level	Reachable	Visible	Firing	Total
A	Above left vocal fold	Low	1	1	1	**3**
B	Below left vocal fold	High	1	1	1	**3**
C	Front juncture of the vocal folds	Medium	1	1	1	**3**
D	Above right vocal fold	High	1	1	1	**3**
E	Ventricle right vocal fold	High	1	1	1	**3**
F	Below right vocal fold	High	1	0	0	**1**

Table 5.2: *Reachability Analysis of the Steerable Optical Fiber*

Target Number	Target Description	Difficulty Level	Reachable	Visible	Firing	Total
A	Above left vocal fold	Low	1	1	1	**3**
B	Below left vocal fold	High	1	1	1	**3**
C	Front juncture of the vocal folds	Medium	1	1	1	**3**
D	Above right vocal fold	High	1	1	1	**3**
E	Ventricle right vocal fold	High	1	1	1	**3**
F	Below right vocal fold	High	1	1	1	**3**

CHAPTER 6

DISCUSSION AND FUTURE OUTLOOK

This chapter presents the conclusions of this doctoral dissertation summarizing the contributions and outlining future directions of research related to this work.

6.1 Concluding Remarks

The main contribution of this thesis to the field of laryngeal laser surgery is the introduction of a new flexible instrument to operate in office settings. We have addressed clinical challenges associated with accessibility, visibility, and reachability. This thesis covers three main thrusts: we addressed clinical challenges in accessing and treating hard-to-reach locations within the larynx. Moreover, we characterized the kinematics of the current medical instrumentation and the new steerable optical fiber to understand the benefits and limitations of each instrument. Finally, we introduced a single-handed controller to integrate the instrument into clinical practice, minimizing alterations to the clinical setting and enabling intuitive operation.

This dissertation successfully demonstrates the application of motion-planning methodologies and ray-casting algorithms to delineate the operation boundaries within the larynx and chart the operational capabilities of our steerable optical fiber within the constrained surgical environments of the larynx. We reported evidence derived from simulations and phantom experiments illustrating the capacity of our instrument to significantly improve surgical access within the larynx. To the best of our knowledge, this research is the first study of a surgical instrument developed specifically for office

procedures in the larynx.

The key findings and contributions of this doctoral research are summarized below:

1. We developed a simulation framework (section 3) as a comprehensive tool to facilitate the identification of hard-to-reach locations within the larynx. The framework enables us to understand anatomical constraints and spatial limitations encountered during surgical interventions. Furthermore, the framework contributes to the characterization of current medical instrumentation used in laryngeal surgery. By simulating surgical scenarios and evaluating the performance of existing instruments, this framework offers valuable insights into the strengths and limitations of conventional tools.

2. We developed and implemented a steerable optical fiber for laryngeal laser surgery (section 4), offering enhanced maneuverability and reach within the confined anatomy of the larynx. Through simulations, we demonstrate that our steerable fiber more than doubles the extent of reachable tissue. Additionally, we demonstrate that we can aim the laser toward hard-to-reach locations, including the 2 cavities immediately above the vocal folds and the under-surface of the vocal fold where is not uncommon that tumors develop.

3. We developed a control unit to provide surgeons with an intuitive interface for single-handle operation of the steerable fiber (section 5). The control unit offers rapid integration into existing clinical workflows minimizing the disruption to the clinical setting. Furthermore, through initial evaluations of the reachable areas within the larynx, we have validated the functionality and performance of our instrument allowing clinicians to have better perceptions and surgical awareness. By enhancing control and visibility, our control unit can improve surgical procedures and extend the pool of candidates to receive in-office laser surgery.

6.2 Future Work

As laryngeal laser surgery continues to evolve, our research holds the potential for clinical translation as well as there is an ongoing need to explore new avenues of innovation. Below, we highlight several significant avenues for future research.

6.2.1 Ergonomic Analysis

Conducting an ergonomic analysis of the single-handle device for office-based laser surgery is crucial to ensure the comfort, safety, and efficacy of surgeons throughout surgical procedures. By assessing factors such as handle design, grip ergonomics, and ease of operation, we aim to optimize the user experience and minimize the risk of musculoskeletal strain and fatigue among surgeons.

6.2.2 Ex-vivo Experiments

Conducting ex-vivo experiments in human larynxes would provide valuable insights into the performance of the steerable optical fiber. The human larynx varies significantly among individuals. Through ex-vivo experiments, researchers and clinicians can be exposed to this variability among anatomical structures to enhance the design of the instrument and then instruct surgeons on implementation strategies for new procedures [75].

6.2.3 Motorized Prototyping

Prototyping a robotic version of the control unit is a potential avenue for research. By integrating motors into the control unit, we anticipate precise maneuverability and control over the steerable optical fiber, enabling surgeons to navigate with increased accuracy and efficiency within the larynx. This alternative approach could represent a significant step forward in advancing office-based surgical techniques. However, it may also suggest a radical shift in the manner in which surgeries are conducted within office settings.

BIBLIOGRAPHY

[1] J. H. Hah, S. Sim, S.-Y. An, M.-W. Sung, and H. G. Choi, "Evaluation of the prevalence of and factors associated with laryngeal diseases among the general population," *The Laryngoscope*, vol. 125, no. 11, pp. 2536–2542, 2015.

[2] S. Y. Jung, M. S. Chun, S. M. Chung, H. S. Kim, *et al.*, "Trends in the incidence and treatment of benign vocal fold lesions in korea, 2006–2015: A nationwide population-based study," *Journal of Voice*, 2018.

[3] N. Bhattacharyya, "The prevalence of voice problems among adults in the united states," *The Laryngoscope*, vol. 124, no. 10, pp. 2359–2362, 2014.

[4] S. M. Cohen, J. Kim, N. Roy, C. Asche, and M. Courey, "Prevalence and causes of dysphonia in a large treatment-seeking population," *The Laryngoscope*, vol. 122, no. 2, pp. 343–348, 2012.

[5] M. Remacle and H. E. Eckel, *Surgery of larynx and trachea*. Springer, 2010.

[6] S. H. Dailey and S. P. Verma, *Laryngeal dissection and surgery guide*. Thieme, 2013.

[7] A. G. Hantzakos and M. Khan, "Office laser laryngology: A paradigm shift," *Ear, Nose & Throat Journal*, pp. Advance Online Publication – doi: 10.1177/0145561320930648, 2020.

[8] S. M. Zeitels and J. A. Burns, "Office-based laryngeal laser surgery with local anesthesia," *Current opinion in otolaryngology & head and neck surgery*, vol. 15, no. 3, pp. 141–147, 2007.

[9] S. M. Zeitels, J. A. Burns, G. Lopez-Guerra, R. R. Anderson, and R. E. Hillman, "Photoangiolytic laser treatment of early glottic cancer: a new management strategy," *Annals of Otology, Rhinology & Laryngology*, vol. 117, no. 7, pp. 2–24, 2008.

[10] A. S. Schimberg, D. J. Wellenstein, E. M. van den Broek, J. Honings, F. J. van den Hoogen, H. A. Marres, R. P. Takes, and G. B. van den Broek, "Office-based vs. operating room-performed laryngopharyngeal surgery: a review of cost differences," *European Archives of Oto-Rhino-Laryngology*, vol. 276, pp. 2963–2973, 2019.

[11] D. J. Wellenstein, H. W. Schutte, R. P. Takes, J. Honings, H. A. Marres, J. A. Burns, and G. B. van den Broek, "Office-based procedures for the diagnosis and treatment of laryngeal pathology," *Journal of Voice*, vol. 32, no. 4, pp. 502–513, 2018.

[12] K. M. Tibbetts and C. B. Simpson, "Office-based 532-nanometer pulsed potassium-titanyl-phosphate laser procedures in laryngology," *Otolaryngologic Clinics of North America*, 2019.

[13] C. J. Rees, G. N. Postma, and J. A. Koufman, "Cost savings of unsedated office-based laser surgery for laryngeal papillomas," *Annals of Otology, Rhinology & Laryngology*, vol. 116, no. 1, pp. 45–48, 2007.

[14] A. T. Hillel, M. C. Ochsner, M. M. Johns III, and A. M. Klein, "A cost and time analysis of laryngology procedures in the endoscopy suite versus the operating room," *The Laryngoscope*, vol. 126, no. 6, pp. 1385–1389, 2016.

[15] S. M. Zeitels, L. M. Akst, J. A. Burns, R. E. Hillman, M. S. Broadhurst, and R. R. Anderson, "Office-based 532-nm pulsed KTP laser treatment of glottal papillomatosis and dysplasia," *Annals of Otology, Rhinology and Laryngology*, vol. 115, no. 9 I, pp. 679–685, 2006.

[16] A. G. Del Signore, R. N. Shah, N. Gupta, K. W. Altman, and P. Woo, "Complications and failures of office-based endoscopic angiolytic laser surgery treatment," *Journal of Voice*, vol. 30, no. 6, pp. 744–750, 2016.

[17] H.-C. Hu, S.-Y. Lin, Y.-T. Hung, and S.-Y. Chang, "Feasibility and associated limitations of office-based laryngeal surgery using carbon dioxide lasers," *JAMA Otolaryngology–Head & Neck Surgery*, vol. 143, no. 5, pp. 485–491, 2017.

[18] E. Ç. Tatar, R. A. Kupfer, J. Y. Barry, C. T. Allen, and A. L. Merati, "Office-based vs traditional operating room management of recurrent respiratory papillomatosis: Impact of patient characteristics and disease severity," *JAMA Otolaryngology–Head & Neck Surgery*, vol. 143, no. 1, pp. 55–59, 2017.

[19] S. M. Hwang, D. Y. Lee, N.-R. Im, H.-J. Lee, B. Kim, K.-Y. Jung, T. H. Kim, and S.-K. Baek, "Office-based laser surgery for benign laryngeal lesion," *Medical Lasers; Engineering, Basic Research, and Clinical Application*, vol. 4, no. 2, pp. 65–69, 2015.

[20] P. J. Swaney, P. A. York, H. B. Gilbert, J. Burgner-Kahrs, and R. J. Webster III, "Design, fabrication, and testing of a needle-sized wrist for surgical instruments," *Journal of medical devices*, vol. 11, no. 1, p. 014501, 2017.

[21] L. Fichera, N. P. Dillon, D. Zhang, I. S. Godage, M. A. Siebold, B. I. Hartley, J. H. Noble, P. T. Russell, R. F. Labadie, and R. J. Webster, "Through the eustachian tube and beyond: A new miniature robotic endoscope to see into the middle ear.," *IEEE robotics and automation letters*, vol. 2, no. 3, pp. 1488–1494, 2017.

[22] "Recurrent respiratory papillomatosis or laryngeal papillomatosis | nidcd." Available at https://www.nidcd.nih.gov/health/recurrent-respiratory-papillomatosis (2019/05/27).

[23] C. S. Derkay and A. E. Bluher, "Update on recurrent respiratory papillomatosis," *Otolaryngologic Clinics of North America*, 2019.

[24] R. Ivancic, H. Iqbal, B. deSilva, Q. Pan, and L. Matrka, "Current and future management of recurrent respiratory papillomatosis," *Laryngoscope investigative otolaryngology*, vol. 3, no. 1, pp. 22–34, 2018.

[25] L. A. Parker, M. Kunduk, D. Blouin, L. Adkins, and A. J. McWhorter, "Voice Outcomes Following Multiple Surgeries for Recurrent Respiratory Papillomatosis," *Journal of Voice*, 2019.

[26] T. Omland, H. Akre, K. A. Lie, P. Jebsen, L. Sandvik, and K. Brøndbo, "Risk factors for aggressive recurrent respiratory papillomatosis in adults and juveniles," *PloS one*, vol. 9, no. 11, p. e113584, 2014.

[27] H. W. Chesson, S. E. Forhan, S. L. Gottlieb, and L. E. Markowitz, "The potential health and economic benefits of preventing recurrent respiratory papillomatosis through quadrivalent human papillomavirus vaccination," *Vaccine*, vol. 26, no. 35, pp. 4513–4518, 2008.

[28] S. M. Zeitels, J. A. Burns, R. A. Franco Jr, R. E. Hillman, S. H. Dailey, and R. R. Anderson, "Office-based treatment of glottal dysplasia and papillomatosis with the

585-nm pulsed dye laser and local anesthesia," *Annals of Otology, Rhinology & Laryngology*, vol. 113, no. 4, pp. 265–276, 2004.

[29] J. A. Koufman, C. J. Rees, W. D. Frazier, L. A. Kilpatrick, S. C. Wright, S. L. Halum, and G. N. Postma, "Office-based laryngeal laser surgery: a review of 443 cases using three wavelengths," *Otolaryngology—Head and Neck Surgery*, vol. 137, no. 1, pp. 146–151, 2007.

[30] D. A. Mouadeb and P. C. Belafsky, "In-office laryngeal surgery with the 585nm pulsed dye laser (pdl)," *Otolaryngology—Head and Neck Surgery*, vol. 137, no. 3, pp. 477–481, 2007.

[31] J. Burns, A. Friedman, M. Lutch, R. Hillman, and S. Zeitels, "Value and utility of 532 nanometre pulsed potassium-titanyl-phosphate laser in endoscopic laryngeal surgery," *The Journal of Laryngology & Otology*, vol. 124, no. 4, pp. 407–411, 2010.

[32] A. Centric, A. Hu, Y. D. Heman-Ackah, V. Divi, and R. T. Sataloff, "Office-based pulsed-dye laser surgery for laryngeal lesions: a retrospective review," *Journal of Voice*, vol. 28, no. 2, pp. 262–e9, 2014.

[33] C. J. Rees, S. L. Halum, R. C. Wijewickrama, J. A. Koufman, and G. N. Postma, "Patient tolerance of in-office pulsed dye laser treatments to the upper aerodigestive tract," *Otolaryngology - Head and Neck Surgery*, vol. 134, no. 6, pp. 1023–1027, 2006.

[34] H. C. Lee, N. E. Pacheco, L. Fichera, and S. Russo, "When the end effector is a laser: A review of robotics in laser surgery," *Advanced Intelligent Systems*, vol. 4, no. 10, p. 2200130, 2022.

[35] T. D. Patel, K. A. Echanique, C. Yip, W. D. Hsueh, S. Baredes, R. C. W. Park, and J. A. Eloy, "Supraglottic squamous cell carcinoma: a population-based study of 22,675 cases," *The Laryngoscope*, vol. 129, no. 8, pp. 1822–1827, 2019.

[36] K. Rabenorosoa, B. Tasca, A. Zerbib, P. Rougeot, N. Andreff, and T. E. Pengwang, "Squipabot: A mesoscale parallel robot for a laser phonosurgery," *International Journal of Optomechatronics*, vol. 9, no. 4, pp. 310–324, 2015.

[37] R. Renevier, B. Tamadazte, K. Rabenorosoa, L. Tavernier, and N. Andreff, "Endoscopic laser surgery: Design, modeling, and control," *IEEE/ASME Transactions on Mechatronics*, vol. 22, no. 1, pp. 99–106, 2016.

[38] P. A. York, R. Peña, D. Kent, and R. J. Wood, "Microrobotic laser steering for minimally invasive surgery," *Science Robotics*, vol. 6, no. 50, p. eabd5476, 2021.

[39] A. Acemoglu, D. Pucci, and L. S. Mattos, "Design and control of a magnetic laser scanner for endoscopic microsurgeries," *IEEE/ASME Transactions on Mechatronics*, vol. 24, no. 2, pp. 527–537, 2019.

[40] D. Kundrat, R. Graesslin, A. Schoob, D. T. Friedrich, M. O. Scheithauer, T. K. Hoffmann, T. Ortmaier, L. A. Kahrs, and P. J. Schuler, "Preclinical Performance Evaluation of a Robotic Endoscope for Non-Contact Laser Surgery," *Annals of Biomedical Engineering*, pp. 1–16, 8 2020.

[41] M. Zhao, T. J. O. Vrielink, A. A. Kogkas, M. S. Runciman, D. S. Elson, and G. P. Mylonas, "Laryngotors: A novel cable-driven parallel robotic system for transoral laser phonosurgery," *IEEE Robotics and Automation Letters*, vol. 5, no. 2, pp. 1516–1523, 2020.

[42] G. Fang, M. C. Chow, J. D. Ho, Z. He, K. Wang, T. Ng, J. K. Tsoi, P.-L. Chan, H.-C. Chang, D. T.-M. Chan, *et al.*, "Soft robotic manipulator for intraoperative mri-guided transoral laser microsurgery," *Science Robotics*, vol. 6, no. 57, p. eabg5575, 2021.

[43] J. Burgner-Kahrs, C. D. Rucker, and H. Choset, "Continuum robots for medical applications: A survey," *IEEE Transactions on Robotics*, vol. 31, no. 6, pp. 1261–1280, 2015.

[44] E. Amanov, T.-D. Nguyen, and J. Burgner-Kahrs, "Tendon-driven continuum robots with extensible sections—a model-based evaluation of path-following motions," *The International Journal of Robotics Research*, vol. 40, no. 1, pp. 7–23, 2021.

[45] K. Picho, B. Persons, J. F. d'Almeida, N. E. Pacheco, C. Reynolds, and L. Fichera, "Multi jet fusion of nylon-12: A viable method to 3d-print concentric tube robots?," *arXiv preprint arXiv:2204.00505*, 2022.

[46] L. Bailly, T. Cochereau, L. Orgeas, N. H. Bernardoni, S. R. Du Roscoat, A. Mcleer-Florin, Y. Robert, X. Laval, T. Laurencin, P. Chaffanjon, *et al.*, "3d multiscale imaging of human vocal folds using synchrotron x-ray microtomography in phase retrieval mode," *Scientific reports*, vol. 8, no. 1, p. 14003, 2018.

[47] R. J. Webster and B. A. Jones, "Design and kinematic modeling of constant curvature continuum robots: A review," *The International Journal of Robotics Research*, vol. 29, no. 13, pp. 1661–1683, 2010.

[48] C. Piazza, J. C. Ribeiro, M. Bernal-Sprekelsen, A. Paiva, and G. Peretti, "Anatomy and physiology of the larynx and hypopharynx," *Otorhinolaryngology, Head and Neck Surgery*, pp. 461–471, 2010.

[49] M. Saran, B. Georgakopoulos, and B. Bordoni, "Anatomy, head and neck, larynx vocal cords," 2018.

[50] K. L. McCullagh, R. N. Shah, and B. Y. Huang, "Anatomy of the larynx and cervical trachea," *Neuroimaging Clinics*, vol. 32, no. 4, pp. 809–829, 2022.

[51] L. Fichera, *Cognitive supervision for robot-assisted minimally invasive laser surgery*. Springer Nature, 2016.

[52] J. Jiang, E. Lin, and D. G. Hanson, "Vocal fold physiology," *Otolaryngologic Clinics of North America*, vol. 33, no. 4, pp. 699–718, 2000.

[53] C. Finck and L. Lejeune, "Structure and oscillatory function of the vocal folds," in *Handbook of Behavioral Neuroscience*, vol. 19, pp. 427–438, Elsevier, 2010.

[54] S. H. Lee, "Surgical anatomy for vocal fold injection," *Vocal Fold Injection*, pp. 17–22, 2021.

[55] "Taking care of your voice | nidcd." Available at https://www.nidcd.nih.gov/health/taking-care-your-voice (2021/04/15).

[56] K. W. Altman, "Vocal fold masses," *Otolaryngologic Clinics of North America*, vol. 40, no. 5, pp. 1091–1108, 2007.

[57] L. S. Mattos, A. Acemoglu, A. Geraldes, A. Laborai, A. Schoob, B. Tamadazte, B. Davies, B. Wacogne, C. Pieralli, C. Barbalata, *et al.*, "μralp and beyond: Micro-technologies and systems for robot-assisted endoscopic laser microsurgery," *Frontiers in Robotics and AI*, p. 240, 2021.

[58] S. Patel, M. Rajadhyaksha, S. Kirov, Y. Li, and R. Toledo-Crow, "Endoscopic laser scalpel for head and neck cancer surgery," in *Photonic Therapeutics and Diagnostics VIII*, vol. 8207, pp. 341–351, SPIE, 2012.

[59] R. E. Goldman, A. Bajo, L. S. MacLachlan, R. Pickens, S. D. Herrell, and N. Simaan, "Design and performance evaluation of a minimally invasive telerobotic platform for transurethral surveillance and intervention," *IEEE transactions on biomedical engineering*, vol. 60, no. 4, pp. 918–925, 2012.

[60] D. V. A. Nguyen, C. Girerd, Q. Boyer, P. Rougeot, O. Lehmann, L. Tavernier, J. Szewczyk, and K. Rabenorosoa, "A hybrid concentric tube robot for cholesteatoma laser surgery," *IEEE Robotics and Automation Letters*, vol. 7, no. 1, pp. 462–469, 2021.

[61] R. M. Murray, S. S. Sastry, and L. Zexiang, "A mathematical introduction to robotic manipulation," 1994.

[62] L. E. Kavraki and S. M. LaValle, "Motion planning," in *Springer Handbook of Robotics*, pp. 139–162, Springer, 2016.

[63] T. Möller and B. Trumbore, "Fast, minimum storage ray-triangle intersection," *Journal of Graphics Tools*, vol. 2, no. 1, pp. 21–28, 1997.

[64] P. Cignoni, M. Callieri, M. Corsini, M. Dellepiane, F. Ganovelli, and G. Ranzuglia, "Meshlab: an open-source mesh processing tool.," in *Eurographics Italian chapter conference*, vol. 2008, pp. 129–136, Salerno, 2008.

[65] "ENT Speech | PENTAX Medical (EMEA)." `https://www.pentaxmedical.com/pentax/en/95/1/Video-Naso-Pharyngo-Laryngoscope-VNL-1570STK`. [Online; accessed 06-April-2024].

[66] C. Baykal, L. G. Torres, and R. Alterovitz, "Optimizing design parameters for sets of concentric tube robots using sampling-based motion planning," in *2015 IEEE/RSJ International Conference on Intelligent Robots and Systems (IROS)*, pp. 4381–4387, IEEE, 2015.

[67] J. Gafford, M. Freeman, L. Fichera, J. Noble, R. Labadie, and R. J. Webster, "Eyes in ears: a miniature steerable digital endoscope for trans-nasal diagnosis of middle ear disease," *Annals of Biomedical Engineering*, vol. 49, no. 1, pp. 219–232, 2021.

[68] A. J. Chiluisa, F. J. Van Rossum, J. B. Gafford, R. F. Labadie, R. J. Webster, and L. Fichera, "Computational optimization of notch spacing for a transnasal ear endoscopy continuum robot," in *2020 International Symposium on Medical Robotics (ISMR)*, pp. 188–194, IEEE, 2020.

[69] A. Bajo, L. M. Dharamsi, J. L. Netterville, C. G. Garrett, and N. Simaan, "Robotic-assisted micro-surgery of the throat: The trans-nasal approach," in *2013 IEEE International Conference on Robotics and Automation*, pp. 232–238, IEEE, 2013.

[70] O. Ferhanoglu, M. Yildirim, K. Subramanian, and A. Ben-Yakar, "A 5-mm piezo-scanning fiber device for high speed ultrafast laser microsurgery," *Biomedical optics express*, vol. 5, no. 7, pp. 2023–2036, 2014.

[71] M. Zhu, Y. Shen, A. J. Chiluisa, J. Song, L. Fichera, and Y. Liu, "Optical fiber coupling system for steerable endoscopic instruments," in *2021 43rd Annual International Conference of the IEEE Engineering in Medicine & Biology Society (EMBC)*, pp. 4871–4874, IEEE, 2021.

[72] P. A. York, P. J. Swaney, H. B. Gilbert, and R. J. Webster, "A wrist for needle-sized surgical robots," in *2015 IEEE International Conference on Robotics and Automation (ICRA)*, pp. 1776–1781, May 2015.

[73] K. W. Eastwood, H. Azimian, B. Carrillo, T. Looi, H. E. Naguib, and J. M. Drake, "Kinetostatic design of asymmetric notch joints for surgical robots," in *2016 IEEE/RSJ International Conference on Intelligent Robots and Systems (IROS)*, pp. 2381–2387, IEEE, 2016.

[74] A. J. Chiluisa, N. E. Pacheco, H. S. Do, R. M. Tougas, E. V. Minch, R. Mihaleva, Y. Shen, Y. Liu, T. L. Carroll, and L. Fichera, "Light in the larynx: a miniaturized robotic optical fiber for in-office laser surgery of the vocal folds," in *2022 IEEE/RSJ International Conference on Intelligent Robots and Systems (IROS)*, pp. 427–434, IEEE, 2022.

[75] M. A. Holm and P. A. Iaizzo, "Importance of human cadaver studies in education and medical device research: Insights derived from various imaging studies and modalities," in *Engineering in Medicine*, pp. 255–280, Elsevier, 2019.